

Review

Methane Oxidation over the Zeolites-Based Catalysts

Linke Wu, Wei Fan, Xun Wang, Hongxia Lin, Jinxiong Tao, Yuxi Liu, Jiguang Deng, Lin Jing and Hongxing Dai *

Beijing Key Laboratory for Green Catalysis and Separation, Key Laboratory of Beijing on Regional Air Pollution Control, Key Laboratory of Advanced Functional Materials, Laboratory of Catalysis Chemistry and Nanoscience, Department of Chemical Engineering, Faculty of Environment and Life, Beijing University of Technology, Education Ministry of China, Beijing 100124, China

* Correspondence: hxdai@bjut.edu.cn; Tel.: +86-10-6739-6118; Fax: +86-10-6739-1983

Abstract: Zeolites have ordered pore structures, good spatial constraints, and superior hydrothermal stability. In addition, the active metal elements inside and outside the zeolite framework provide the porous material with adjustable acid–base property and good redox performance. Thus, zeolites-based catalysts are more and more widely used in chemical industries. Combining the advantages of zeolites and active metal components, the zeolites-based materials are used to catalyze the oxidation of methane to produce various products, such as carbon dioxide, methanol, formaldehyde, formic acid, acetic acid, and etc. This multifunction, high selectivity, and good activity are the key factors that enable the zeolites-based catalysts to be used for methane activation and conversion. In this review article, we briefly introduce and discuss the effect of zeolite materials on the activation of C–H bonds in methane and the reaction mechanisms of complete methane oxidation and selective methane oxidation. Pd/zeolite is used for the complete oxidation of methane to carbon dioxide and water, and Fe- and Cu-zeolite catalysts are used for the partial oxidation of methane to methanol, formaldehyde, formic acid, and etc. The prospects and challenges of zeolite-based catalysts in the future research work and practical applications are also envisioned. We hope that the outcome of this review can stimulate more researchers to develop more effective zeolite-based catalysts for the complete or selective oxidation of methane.

Keywords: zeolite-based catalyst; methane combustion; selective methane oxidation; acid–base property; reaction mechanism



Citation: Wu, L.; Fan, W.; Wang, X.; Lin, H.; Tao, J.; Liu, Y.; Deng, J.; Jing, L.; Dai, H. Methane Oxidation over the Zeolites-Based Catalysts.

Catalysts **2023**, *13*, 604. <https://doi.org/10.3390/catal13030604>

Academic Editor: Giuseppe Pantaleo

Received: 13 February 2023

Revised: 9 March 2023

Accepted: 13 March 2023

Published: 16 March 2023



Copyright: © 2023 by the authors. Licensee MDPI, Basel, Switzerland. This article is an open access article distributed under the terms and conditions of the Creative Commons Attribution (CC BY) license (<https://creativecommons.org/licenses/by/4.0/>).

1. Introduction

Methane is the major constituent of natural gas, which consists of approximately 70 to 90% [1]. Methane is the simplest saturated hydrocarbon with the lowest C/H molar ratio, and its burning with oxygen can produce a huge amount of energy ($\Delta H = -891$ kJ/mol) [2,3]. In the transformation of the global economy from oil-based energy production to renewable energy production, natural gas consumption has increased dramatically in the past few years due to the huge reserve of natural gas on the Earth [4]. Since methane is mainly stored in sparsely populated areas, its emission will inevitably occur in the processing of coal, gas, and oil extraction [5]. At the same time, methane can also produce biogas through anaerobiological oxidation with crops, waste, and residues [6]. As we all know, the temperature of methane combustion can reach above 1200 °C, which will cause the oxidation of nitrogen with oxygen in the air to generate NO_x at high temperatures [7]. In addition, the incomplete combustion of methane can also form CO, which is seriously harmful to the atmosphere [8]. Furthermore, methane is of a very stable structure and exerts 20 times higher greenhouse effect than CO_2 emissions [9]. On the one hand, methane has been regarded as a high-efficiency fuel [10]; on the other hand, methane can also be used for selective oxidation to produce syngas and various value-added chemicals (e.g., methanol [11], formic acid [12], and acetic acid [13,14], and etc.).

As we all know, there are many kinds of catalysts used for methane oxidation, such as noble metal catalysts, metal oxide catalysts, zeolite-based catalysts, and etc. Noble metal catalysts exhibit high catalytic activities, high selectivities, and good anti-poisoning performance, but high cost limits their wide applications. Although metal oxide catalysts are cheap and less harmful to the environment, their activities and selectivities are low and easy to be deactivated. However, zeolites with large specific surface areas, regular microporous channels, good activity stability, hydrothermal stability, and controllable acid–base property, which are widely used in industrial applications due to their excellent catalytic activities and product selectivities [15,16]. For instance, Y-type zeolites are widely utilized in catalytic cracking of petroleum [17], ZSM-5 is often used to improve the octane number of gasoline, and SPAO-34 is commonly used for the conversion of low-carbon olefins, methanol-to-olefin process and NH_3 -SCR of NO_x [18–21]. Up to now, there have been a number of review articles on methane conversions in the literature, such as methane aromatization [22,23], methane oxidation over transition-metal oxides [24,25], oxidation of methane by the composite metal oxides [26,27], metal organic framework-based catalysts for methane oxidation [28], and single-atom catalysts for methane oxidation [29]. In recent years, zeolites have been extensively utilized in methane oxidation due to their excellent catalytic performance and stability [30]. Many researchers prepared a number of zeolite-based noble metal catalysts (e.g., Pd/H-MOR [31], Pd/HZSM-5 [32], Pd-Ce/HZSM-5 [33], Pd@Silicilite-1 [34], and PdPt/TiO₂/ZSM-5 [35]) for the complete oxidation of methane. In the meanwhile, some zeolite-based catalysts, such as Pd₁O₄/ZSM-5 [11], Cu-ZSM-5 [36], Fe-SSZ-13 [37], Zn-ZSM-5 [38], and Co-ZSM-5 [39] were investigated for the selective oxidation of methane to methanol, which were found to exhibit good catalytic performance. The above studies have promoted the development of highly stable, selective, and economical catalysts for breaking the C–H bonds of methane in order to produce high-value products and minimize the impact on climate.

In this review article, we briefly introduce the applications of zeolites-based catalysts, methane oxidation mechanisms, and methane oxidation significance and challenges in the future work. Furthermore, the structure–performance relationships of these zeolites-based catalysts are also discussed. It is envisioned that this review article can promote the future developments of methane oxidation over the zeolites-based catalysts to meet the emerging demands for practical applications of methane utilization.

2. Methane Oxidation

2.1. Complete Oxidation of Methane

Currently, the development of the complete oxidation of methane was mainly used for processing the incomplete combustion of methane from the exhaust gas of natural gas engines, which can effectively reduce the greenhouse effect caused by incomplete combustion of methane [40]. Catalytic combustion of methane is a complete oxidation reaction on the surface of a catalyst, which is mainly a flameless combustion process. Compared with the traditional flame combustion, catalytic methane combustion can reduce the ignition temperature of fuel using a catalyst, improve the combustion efficiency of methane, and reduce the generation of atmospheric pollutants. The Pd/zeolite catalysts are commonly used for the complete oxidation of methane, which shows excellent catalytic performance [41]. By tuning the pore structures, acidic and alkaline properties, crystal sizes, morphologies, and hydrophobicity or hydrophilicity of the zeolites, we can effectively design and prepare the zeolite-based materials with excellent catalytic performance. Table 1 summarizes the operation conditions and catalytic activities of the typical zeolite-based catalysts for the combustion of methane.

Table 1. Summary of operation conditions and catalytic activities of the typical zeolite-based catalysts for the combustion of methane.

Catalyst	Metal Loading (wt%)	Topology	Reaction Condition	Catalytic Activity	Stability	Ref.
Pd/H-MOR	1.01 wt% Pd	MOR	1 vol% CH ₄ , 4 vol% O ₂ , N ₂ (balance), GHSV = 70,000 h ⁻¹	T _{98%} = 475 °C	–	[31]
Pd/Na-MOR	0.99 wt% Pd	MOR	1 vol% CH ₄ , 4 vol% O ₂ , N ₂ (balance), GHSV = 70,000 h ⁻¹	T _{98%} = 425 °C	Kept stable during 90 h of on-stream reaction	[31]
Pd/HZSM-5	2.05 wt% Pd	MFI	1 vol% CH ₄ , 4 vol% O ₂ , N ₂ (balance), GHSV = 15,000 h ⁻¹	T _{98%} = 450 °C	No deactivation within 10 h of reaction	[32]
Pd-Ce/HZSM-5	0.95 wt% Pd	MFI	2 vol% CH ₄ , 8 vol% O ₂ , N ₂ (balance), GHSV = 48,000 h ⁻¹	T _{98%} = 375 °C	Kept stable during 30 h of on-stream reaction	[33]
Pd@Silicalite-1	0.98 wt% Pd	MFI	1 vol% CH ₄ , 20 vol% O ₂ , N ₂ (balance), GHSV = 24,000 h ⁻¹	T _{90%} = 309 °C	Kept stable during 100 h of on-stream reaction	[34]
PdPt/TiO ₂ /ZSM-5	5.31 wt% Pd 2.21 wt% Pt	MFI	1 vol% CH ₄ , 10 vol% O ₂ , Ar (balance), GHSV = 24,000 h ⁻¹	T _{90%} = 319 °C	Kept stable during 35 h of on-stream reaction	[35]
Rh/ZSM-5	1.95 wt% Pd	MFI	2500 ppm CH ₄ , 10 vol% O ₂ , N ₂ (balance), GHSV = 150,000 h ⁻¹	T _{98%} = 420 °C	Kept stable during 20 h of on-stream reaction	[42]
Pd/ZSM-5	0.93 wt% Pd	MFI	1 vol% CH ₄ , 4 vol% O ₂ , N ₂ (balance), GHSV = 70,000 h ⁻¹	T _{98%} = 410 °C	Kept stable during 80 h of on-stream reaction	[43]
PdO/Beta	0.7 wt% Pd	–	1 vol% CH ₄ , 20 vol% O ₂ , N ₂ (balance), GHSV = 30,000 h ⁻¹	T _{98%} = 350 °C	Kept stable after 6 cycle tests	[44]
Pd@Silicalite-1	0.83 wt% Pd	MFI	0.5 vol% CH ₄ , 20 vol% O ₂ , N ₂ (balance), GHSV = 20,000 h ⁻¹	T _{98%} = 360 °C	Kept stable during 200 h of on-stream reaction	[45]
PdCo@ZSM-5	0.54 wt% Pd 0.091 wt% Co	MFI	1 vol% CH ₄ , 20 vol% O ₂ , N ₂ (balance), GHSV = 60,000 h ⁻¹	T _{98%} = 385 °C	Kept stable during 20 h of on-stream reaction	[46]
Na-FAU-Pd	5.65 wt% Pd	FAU	5 vol% CH ₄ , 10 vol% O ₂ , He (balance), GHSV = 40,000 h ⁻¹	T _{98%} = 245 °C	–	[47]

Friberg and coworkers prepared the Pd/H-beta and Pd/H-SSZ-13 catalysts with different Si/Al ratios [48]. The experimental results showed that the type of zeolite framework and the different Si/Al ratio exerted important influences on the catalytic activity and Pd chemical valence. When the Al content decreases, the hydrophobicity of the zeolite increases, and the conversion and stability of the catalyst are significantly improved in methane oxidation. The authors thought that the selection of the zeolite support was essential to minimize the formation of the ion-exchange Pd²⁺ species, and to form well-dispersed Pd particles for the highly active oxidation of methane. Operando X-ray absorption spectroscopic (XAS) results revealed that, when switching between the pulses of (CH₄/Ar) and lean (CH₄/O₂/Ar) atmospheres, the catalysts with high methane oxidation activity exhibited a rapid transition between metallic Pd⁰ and oxidized Pd²⁺. It was also found that

high silica beta-zeolite supported with low cation-exchange capacity limited the formation of large palladium particles and ion-exchanged palladium, thus resulting in the drop in methane conversion. A similar phenomenon was also observed over the Pd/Na-MOR catalysts [31]. The research results demonstrated that, when sodium ions were removed, acid sites were produced in the zeolite, which could effectively inhibit the mobility of palladium and keep palladium highly dispersed. Therefore, stable methane conversions were maintained for over 90 h under the hydrothermal conditions. As can be demonstrated by the XAS measurements, the catalyst maintained a high transient activity, and the increases of palladium oxide and oxygen vacancies provided a higher steady-state methane oxidation activity during the oxidation process. Christensen and coworkers found that the zeolites with different Si/Al ratios could also affect the existence of noble metals [42], in which they prepared a series of ZSM-5 (MFI-type) zeolites with Si/Al = 15–280 and an SSZ-13 (CHA-type) zeolite with Si/Al = 12, which were studied as support materials for Rh in order to investigate the distributions of the different Rh sites. The authors found that Rh existed in the form of Rh₂O₃ particles, with the zeolite being of the highest silicon content. While on the zeolite support with a high aluminum content, Rh was dispersed at the zeolite-exchange site in the form of a single atom. According to the activity evaluation data, it could be realized that the ZSM-5 (280) with the highest silicon content showed the good catalytic activity ($T_{98\%} = 420$ °C at a space velocity of 150,000 mL/(g h)). It was also revealed that Rh existed in the form of oxide nanoparticles, with the catalyst exhibiting better catalytic activity under the stable conditions.

The isomorphic substitution of the zeolite framework is also an effective means to improve the activity of a zeolite catalyst. Muramatsu and coworkers [49] prepared Ga-substituted MFI-type zeolites with different Si/Ga ratios using the ball milling and hydrothermal two-step synthesis methods. Compared with the traditional silicalite-1 catalyst, the one with a higher amount of the active oxygen species showed a better catalytic activity and selectivity. In addition, Lim et al. [40] investigated effects of different cage systems (i.e., CHA, LTA, UFI, RTH, and MFI) on the methane combustion activity of Pd/zeolites. The experimental results demonstrated that Pd/SSZ-13 possessed the highest acidity and catalytic activity among the other zeolite-structured catalysts. The strong acid strength of SSZ-13 could produce a strong interaction between the PdO species and zeolite skeleton, thus effectively inhibiting not only PdO sintering, but also de-aluminization in methane combustion. Although the Pd/zeolite catalysts show good activities, Pd nanoparticles are easy to be sintered during the methane combustion process. A large amount of water vapor is generated in methane catalytic combustion, which will lead to partial deactivation of the catalyst. Petrov and coworkers [43] prepared mesoporous hierarchical Pd/Na-ZSM-5 catalysts modified with different acids (e.g., hydrochloric, nitric, and oxalic acids), and found that the treatment with oxalic acid or nitric acid could selectively remove the framework aluminum from the zeolite, which also significantly improved the activity and stability of the Pd/Na-ZSM-5 catalyst ($T_{98\%} = 410$ °C at a space velocity of 70,000 mL/(g h)). The mesoporous formed by dealumination of the zeolite could effectively fix the palladium nanoparticles, thus effectively preventing growth and sintering of the nanoparticles. Furthermore, such a dealumination improved the stability of the zeolitic framework, which was helpful to further enhance the performance of the catalyst. They also confirmed that, after adjustment of the synthesis conditions, the approach could be applied to other zeolite structures, for instance, beta and mordenite zeolites.

In addition, Cargnello and coworkers [50] prepared nineteen Pd/zeolite catalysts with different hydrophobic or hydrophilic properties, and investigated their roles in catalytic methane combustion. According to the kinetic study, they found that, when the hydrophobicity or hydrophilicity of the zeolite was optimized, water resistance of the Pd catalyst used for methane combustion was significantly improved. The operando diffuse reflection infrared Fourier transform spectroscopic (DRIFTS) study substantiated that, through the adsorption/desorption process, water was effectively removed from the surface of the active PdO phase at the acid site of the zeolite. Some researchers also prepared PdO/beta [44]

and Pd@silicalite [45,51] catalysts for methane combustion. They found that using the in situ seed-directed synthesis method to prepare the Pd/zeolite catalysts could form a strong interaction between precious metals and zeolite, which enhanced methane adsorption on the catalyst, so that the catalyst showed excellent stability and efficient catalytic methane combustion. Gao et al. [52] prepared the Pd@H-ZSM-5 catalyst, in which the isolated Pd²⁺ species were stably encapsulated in the zeolite using the in situ hydrothermal method. The results revealed that the presence of the Brønsted acid sites was conducive to methane adsorption and promoted its activation at the adjacent Pd sites, generating an effective synergy between Pd sites and Brønsted acid sites in the confined space of the MFI zeolite. In situ near atmospheric X-ray photoelectron spectroscopy (XPS) analysis results showed that there was a reversible redox cycle of Pd²⁺ → Pdⁿ⁺ → Pd²⁺ in the catalytic methane combustion process. In addition, Guo and his or her colleagues also studied the bimetallic oxide catalysts supported on zeolites [46], in which they prepared the PdCo@MFI catalyst via a one-pot route. The results demonstrated that the MFI zeolite framework remained intact in PdCo@MFI, and the 0.4–0.6 nm PdCo bimetallic oxide clusters were preferentially located in the sinusoidal channel of the MFI. In addition, introduction of the Co species promoted the activation of the surface oxygen species and modulated electronic state of the Pd species, effectively improving the catalytic performance at the lowest methane complete conversion temperature in the presence of water vapor ($T_{98\%} = 385\text{ °C}$ at a space velocity of 60,000 mL/(g h)).

There have been some references on confining the bimetallic clusters in the zeolite catalysts for the complete oxidation of methane. In order to promote industrial applications of the catalysts, Tan et al. used the sucrose-modified steam-assisted crystallization method to generate the Pd/silicalite-1 catalysts, which were covered on the cordierite surface for the low-temperature oxidation of methane [53]. It was found that the crystal size of a zeolite decreased with the increase in sucrose solution content. When 4 mol% sucrose solution was added to the reaction system, the size of silicalite-1 changed from 2–8 nm to 200–250 nm, and further addition of sucrose reduced the crystallinity, specific surface area, and micropore volume of the zeolite. The nano zeolite coating possessed good mechanical stability, and the palladium catalyst supported on the silicalite-1-coated cordierite showed good stability and catalytic activity for methane oxidation, which provided a new strategy for industrial catalytic methane combustion applications of the catalysts. In addition, Tosheva and coworkers prepared the Na-FAU-Pd and H-FAU-Pd zeolites using traditional silica sol and silica sol extracted from geothermal fluid extract as silicon source [47], respectively. All of the catalysts show catalytic activity in the oxidative decomposition of methane, and the zeolites containing sodium performed the best. Among them, the catalysts prepared from the natural silicon sources and the ones derived from the traditional silicon sources have similar catalytic activities. The results demonstrate that using a freely available natural resource as a silicon source to prepare the zeolite-based catalysts can further promote the industrial development of these materials.

In short, the synergism between the Pd species and zeolite makes the Pd-based zeolite catalyst show high catalytic performance in methane oxidation. At the same time, the special structure of the zeolite carrier can limit the deactivation of the active Pd components, thus maintaining the stability in catalytic activity. The introduction of Co and Ce species promotes the activation of O₂ to the surface oxygen species, regulates the electronic state of the Pd species, which can also promote formation of the PdO species and catalyze the oxidation of methane at low temperatures. However, the Brønsted acid sites in the catalysts also play an important role in methane oxidation. In the Pd-based zeolite catalysts, the Brønsted site can improve the activity of methane oxidation. On the one hand, the existence of the Brønsted acid sites can not only increase the number of adsorption sites on the catalyst surface, but also generate the adsorbed oxygen species from oxygen molecules, which makes it easier for oxygen molecules to participate in the reaction, thus promoting the adsorption and activation of oxygen, improving the migration rate of oxygen molecules, and making methane oxidation be easier. On the other hand, Brønsted acid sites on the

catalyst surface can activate methane by forming hydrogen bonds with methane, making it easier to combine with oxygen molecules to form the active species and improve its reactivity. It should be noted that the existence of the Brønsted acid sites exerts a great impact on the catalytic activity and selectivity of the catalysts. Too many acid sites will lead to too strong acidity of the catalysts, hence decreasing its selectivity and activity. Therefore, when preparing, it is necessary to control the number and distribution of the Brønsted acid sites in the Pd-based zeolite catalysts to ensure their excellent catalytic performance in methane conversion.

2.2. Reaction Mechanism of Complete Oxidation of Methane

At present, three types of catalytic methane combustion mechanisms and kinetic models have been proposed, including the Langmuir–Hinshelwood mechanism (L–H), Eley–Rideal mechanism (E–R), and Mar-van Krevelen mechanism (MvK) [54,55].

The L–H mechanism is that two kinds of gas phase reactants are adsorbed on the catalyst surface and interact each other, and the formed products are desorbed from the catalyst surface, thus completing the catalytic reaction [56]. At low temperatures, the complete oxidation of methane usually takes place via the L–H mechanism. The L–H mechanism uses OH radicals as the active center at low temperatures, and the reaction rate is slow but the selectivity is high. The reaction temperatures in the L–H mechanism are generally in the range of 200–300 °C, and platinum and palladium are usually used as catalysts. In methane combustion, methane and oxygen are first adsorbed on the catalyst surface, and then the adsorbed methane reacts with the adsorbed oxygen species to generate CO₂ and H₂O. Mei and Xue designed a kinetic model for the catalytic combustion of methane over the Pd/H-SSZ-13 catalyst [57]. Density functional theory (DFT) calculations verified that methane combustion conforms the L–H mechanism, indicating that both methane and oxygen adsorbed on the catalyst surface participate in the reaction. As shown in Figure 1A, the process can be described in the following steps (* represents an active adsorption site):

- (1) $O_2 \rightarrow O^*$
- (2) $CH_4 \rightarrow CH_4^*$
- (3) $O^* + CH_4^* \rightarrow CH_3^* + OH^* + O^*$
- (4) $CH_2^* + OH^* + OH^* \rightarrow CH^* + H_2O^* + OH^*$
- (5) $C^* + H_2O^* + OH^* \rightarrow C^* + 2H_2O$
- (6) $C^* + O_2 + 2H_2O \rightarrow C^* + O_2^* + 2H_2O$
- (7) $CO^* + O^* + 2H_2O \rightarrow CO_2^* + 2H_2O$

In addition, methane can also be in turn dissociated into CH₃^{*}, CH₂^{*}, CH^{*}, and C^{*}, and then reacts with the adsorbed oxygen species. Jørgensen and coworkers [58] investigated the mechanism of dehydrogenation of methane to carbon and hydrogen, and found that, under high temperatures, the C^{*} species reacted with the OH^{*} species to generate the COH^{*} species, which were then oxidized by the O^{*} species to the OCOH^{*} species. After that, the OCOH^{*} species were finally oxidized into CO₂ and H₂O. At low temperatures, however, CO₂ was generated by the reaction of C^{*} + O^{*} or CO^{*} + O^{*}, and H₂O was formed through the reaction of O^{*} + H^{*} or OH^{*} + OH^{*}. Huang et al. [59] probed the reaction path of catalytic methane combustion over the Pt₁₃ clusters (Figure 1B), and pointed out that the presence of H₂O could not only change the reaction path, but also facilitate the catalytic oxidation of methane.

The E–R mechanism is a surface reaction mechanism in the complete oxidation of methane. The active center is the adsorption species on the catalyst surface and the oxidation–reduction reaction between the oxidant and methane molecule. The reaction conditions in the E–R mechanism are generally in the medium temperature range, and the metal oxide catalysts are usually used as catalysts. The advantage of the E–R mechanism is that it has a wide range of applications and can be used at different temperatures. In the E–R mechanism, methane reacts directly with the adsorbed oxygen species on the catalyst surface, and then produces CO₂ and H₂O. Xu et al. [60] illustrated that the E–R mechanism

was adequate to describe the experiment data. Oxygen was adsorbed on the surface of the catalyst, excited by the active site to form the oxygen species participating in the reaction, and then the generated oxygen species reacted with the gaseous methane at the active sites to produce CO_2 and H_2O . Saracco and coworkers [61] used the experimental kinetic results to reasonably reveal the E–R mechanism of catalytic methane combustion.

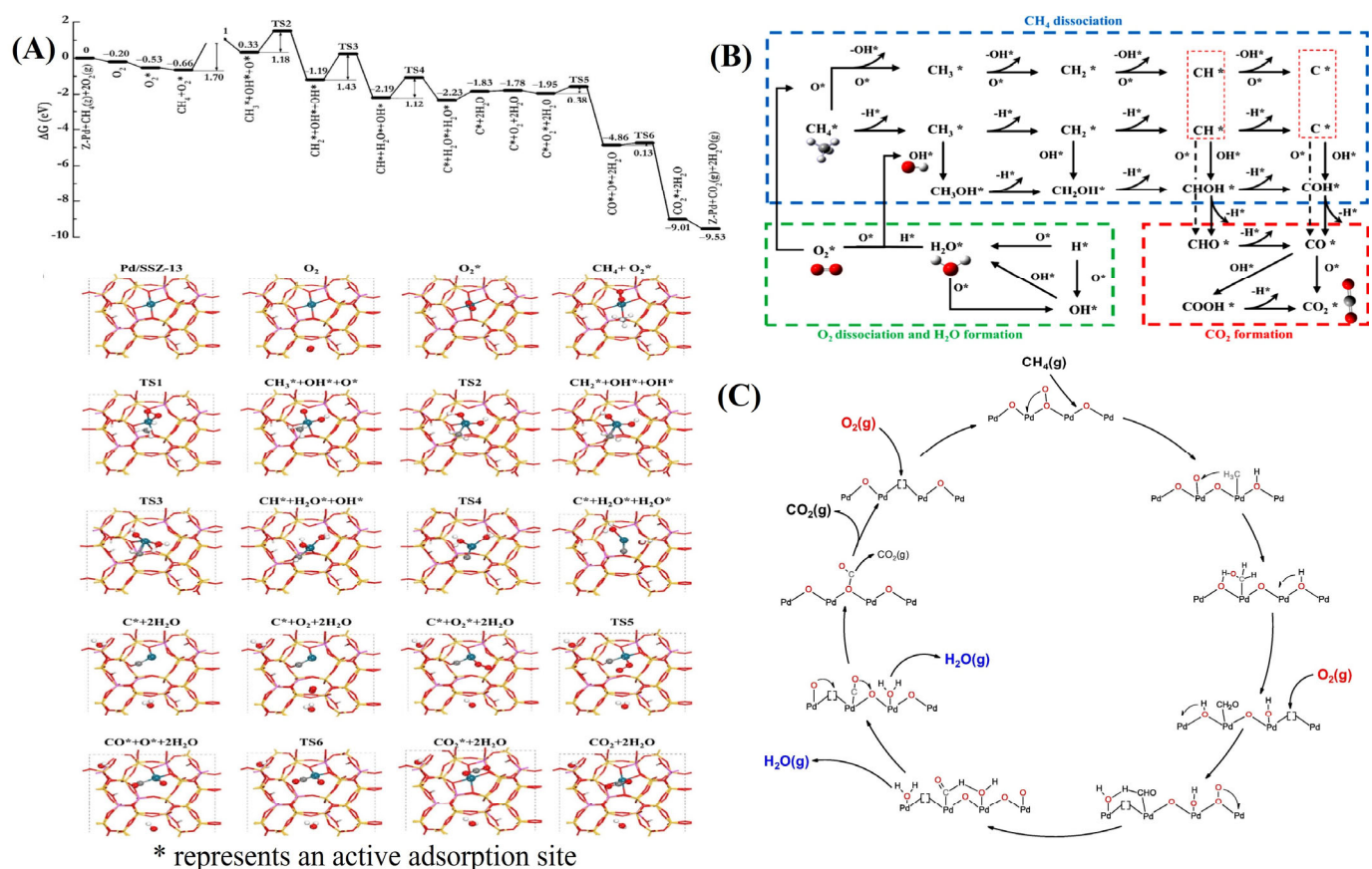


Figure 1. (A) Gibbs free energy profile of CH_4 oxidation over the Pd/H-SSZ-13 and the optimized structures of corresponding reaction intermediates and transition states. Reprinted/adapted with permission from Ref. [57]. Copyright 2022, copyright Elsevier Ltd., (B) feasible reaction pathways in the catalytic combustion of methane. Reprinted/adapted with permission from Ref. [59]. Copyright 2021, copyright Elsevier Ltd., and (C) catalytic cycle of the preferential reaction path following a Mars–van–Krevelen redox mechanism for methane oxidation over PdO (101) under the dry feed conditions (200–400 °C). Reprinted/adapted with permission from Ref. [62]. Copyright 2019, copyright Elsevier Ltd.

In the MvK mechanism, the methane adsorbed on the catalyst surface reacts with lattice oxygen, and the oxygen in the feedstock is adsorbed by the catalyst to fill the oxygen vacancies generated on its surface, forming a cycle of the active oxygen consumption and generation, and finally continuously generating CO_2 and H_2O . At high temperatures, the complete oxidation of methane usually proceeds according to the MvK mechanism. The MvK mechanism uses free radicals (such as CH_3 and HO_2) as the active center at high temperatures, and the reaction rate is fast but the selectivity is low. The reaction temperatures in the MvK mechanism are generally in the range of 800–1000 °C, and the catalysts are usually metal oxide catalysts. Ciuparu et al. [63] did the isotope-labeled pulse experiment to explore the catalytic methane combustion mechanism. The results showed that the oxidation of methane by ^{16}O atoms in PdO was greater than that by ^{18}O atoms adsorbed in the gas phase. In addition, the surface of the catalyst completed the oxidation of methane through the continuous reduction–re-oxidation cycles. Stotz and

coworkers [62] explored the surface reaction kinetics of methane oxidation over the PdO catalyst. As shown in Figure 1C, methane dissociates into CH_3^* , CH_2^* , and H^* , which interacted with lattice oxygen in the catalyst to generate CH_3O^* , CH_2O^* , CO_2 , and H_2O . During the reaction process, oxygen constantly fills the oxygen vacancies formed due to the removal of lattice oxygen. Similar results have also reported by other researchers [50,64,65].

In the catalytic oxidation of methane, methane and oxygen molecules are first adsorbed on the catalyst surface, and then react with each other to generate CO_2 and H_2O . Among the L–H, E–R, and MvK mechanisms, the reaction process is as follows: methane molecules enter the catalyst surface through internal and external diffusion, where the methane molecules adsorbed on the catalyst surface undergo one or more steps of reaction, and are finally oxidized to CO_2 and H_2O by oxygen that is also adsorbed on the catalyst surface or lattice oxygen in the catalyst. After that, the generated CO_2 and H_2O are desorbed from the catalyst surface and returned to the gas phase through diffusion, while the oxygen in the feedstock replenished the oxygen vacancies or adsorbed active oxygen species on the catalyst surface, finally completing the redox process of adsorption, deoxygenation, desorption, and oxygen supplement and regeneration.

2.3. Selective Oxidation of Methane

2.3.1. Selective Oxidation of Methane to Methanol

The selective conversion of methane to sustainable hydrocarbons and oxygenates has attracted much attention. Table 2 summarizes the operation conditions and catalytic activities of the typical zeolite-based catalysts for the selective oxidation of methane. It can be seen from Table 2 that, in the selective oxidation of methane to methanol, when oxygen is used as an oxidant, the selectivity of methanol is higher than that when H_2O_2 , N_2O , or other oxidants are adopted as the oxidant. In addition, similar phenomena also exist in the selective oxidation of methane to formaldehyde. In the selective oxidation of methane to formic acid and acetic acid, however, the selectivity of the product is higher when H_2O_2 is used as an oxidant.

Table 2. Summary of operation conditions and catalytic activities of the typical zeolite-based catalysts for the selective oxidation of methane.

Catalyst	Method	Metal Precursor	Metal Loading (wt%)	Topology	Oxidant	Reaction Temperature (°C)	Desired Product, Yield ($\mu\text{mol/g}_{\text{cat}}$)	Desired Product, Selectivity	Ref.
Cu-ERI	ion-exchanged	$(\text{CH}_3\text{COO})_2\text{Cu}$	4.2 wt% Cu	ERI	O_2	300	CH_3OH , 147	CH_3OH , 95%	[66]
Cu-H-MOR	ion-exchanged	$\text{Cu}(\text{CH}_3\text{COO})_2 \cdot \text{H}_2\text{O}$	0.42 wt% Cu	MOR	O_2	200	CH_3OH , 39	CH_3OH , 90%	[67]
Fe/ZSM-5	wet impregnation	$\text{Fe}(\text{NO}_3)_3 \cdot 9\text{H}_2\text{O}$	0.1 wt% Fe	MFI	H_2O_2	50	CH_3OH , 66	CH_3OH , 90%	[68]
Fe-ferrierite	ion-exchanged	$\text{Fe}(\text{C}_5\text{H}_7\text{O}_2)_3$	2.0 wt% Fe	FER	O_2	300	CH_3OH , 75	CH_3OH , 93%	[69]
Fe-ZSM-5	ion-exchanged	FeSO_4	0.46 wt% Fe	MFI	H_2O_2	50	CH_3OH , 25	CH_3OH , 78%	[70]
Fe-ZSM-5	ion-exchanged	FeCl_2	0.45 wt% Fe	MFI	H_2O_2	50	CH_3OH , 18	CH_3OH , 70%	[70]
Fe-ZSM-5	wet impregnation	FeSO_4	0.54 wt% Fe	MFI	H_2O_2	50	CH_3OH , 13	CH_3OH , 63%	[70]
LaFe-ZSM-5	wet impregnation	$\text{Fe}(\text{NO}_3)_3 \cdot 9\text{H}_2\text{O}$ $\text{La}(\text{NO}_3)_3 \cdot 6\text{H}_2\text{O}$	0.34 wt% Fe 0.18 wt% La	MFI	H_2O_2	50	CH_3OH , 114	CH_3OH , 99%	[71]
Fe-CHA	wet impregnation	$\text{Fe}(\text{C}_5\text{H}_7\text{O}_2)_3$	0.22 wt% Fe	CHA	N_2O	160	CH_3OH , 27	CH_3OH , 87%	[72]
Cu-MOR	ion-exchanged	$\text{Cu}(\text{NO}_3)_2 \cdot 3\text{H}_2\text{O}$	0.95 wt% Cu	MOR	H_2O	200	CH_3OH , 20	CH_3OH , 97%	[73]
Cu-SSZ-13	ion-exchanged	$\text{Cu}(\text{CH}_3\text{COO})_2 \cdot \text{H}_2\text{O}$	0.57 wt% Cu	CHA	O_2	270	CH_3OH , 83	CH_3OH , 98%	[74]
Cu/CHA	ion-exchanged	$\text{Cu}(\text{CH}_3\text{COO})_2 \cdot \text{H}_2\text{O}$	1.05 wt% Cu	CHA	O_2	300	CH_3OH , 54.3	CH_3OH , 91%	[75]
Cu-SSZ-39	ion-exchanged	$(\text{CH}_3\text{COO})_2\text{Cu}$	0.256 wt% Cu	CHA	O_2	450	CH_3OH , 36	CH_3OH , 84%	[76]

Table 2. Cont.

Catalyst	Method	Metal Precursor	Metal Loading (wt%)	Topology	Oxidant	Reaction Temperature (°C)	Desired Product, Yield ($\mu\text{mol/g}_{\text{cat}}$)	Desired Product, Selectivity	Ref.
Cu-SPAO-34	ion-exchanged	$(\text{CH}_3\text{COO})_2\text{Cu}$	0.6 wt% Cu	CHA	O_2	450	CH_3OH , 15	CH_3OH , 71%	[76]
Cu-MOR	ion-exchanged	$\text{Cu}(\text{NO}_3)_2 \cdot 3\text{H}_2\text{O}$	0.6 wt% Cu	MOR	O_2	400	CH_3OH , 31.6	CH_3OH , 98%	[77]
Cu-SSZ-13	ion-exchanged	$(\text{CH}_3\text{COO})_2\text{Cu}$	0.5 wt% Cu	CHA	O_2	200	CH_3OH , 118	CH_3OH , 88%	[78]
Fe-BEA	ion-exchanged	$\text{Fe}(\text{NO}_3)_3 \cdot 9\text{H}_2\text{O}$	1.04 wt% Fe	BEA	N_2O	250	CH_3OH , 227	CH_3OH , 73%	[79]
$\text{FePO}_4/\text{MCM-41}$	wet impregnation	$\text{Fe}(\text{NO}_3)_3$	40 wt% Fe	–	N_2O	550	HCHO, 58	HCHO, 79%	[39]
$\text{FePO}_4/\text{SBA-15}$	wet impregnation	$\text{Fe}(\text{NO}_3)_3$	5.0 wt% Fe	–	O_2	500	HCHO, 46	HCHO, 81%	[80]
Co-ZSM-5	wet impregnation	$\text{Co}(\text{NO}_3)_2 \cdot 6\text{H}_2\text{O}$	10.0 wt% Co	MFI	O_2	360	HCHO, 40	HCHO, 75%	[81]
Mo/ZSM-5	wet impregnation	$(\text{NH}_4)_6\text{Mo}_7\text{O}_{24} \cdot 4\text{H}_2\text{O}$	6.5 wt% Mo	MFI	O_2	600	HCHO, 22	HCHO, 73%	[82]
$\text{VO}_x/\text{SBA-15}$	wet impregnation	NH_4VO_3	1.7 wt% V	–	O_2	600	HCHO, 54	HCHO, 85%	[83]
$\text{VO}_x/\text{MCM-41}$	wet impregnation	NH_4VO_3	3.5 wt% V	–	O_2	550	HCHO, 28	HCHO, 83%	[84]
$\text{CuO}_x/\text{SBA-15}$	wet impregnation	$\text{Cu}(\text{C}_5\text{H}_7\text{O}_2)_2$	0.6 wt% Cu	–	O_2	625	HCHO, 78	HCHO, 71%	[85]
Fe/ZSM-5	Ball-milling	$\text{Fe}(\text{NO}_3)_3 \cdot 9\text{H}_2\text{O}$	0.5 wt% Fe	MFI	H_2O_2	70	HCOOH, 115	HCOOH, 96%	[86]
Fe/ZSM-5	ion-exchanged	$\text{Fe}(\text{NO}_3)_3$	0.03 wt% Fe	MFI	H_2O_2	80	HCOOH, 383	HCOOH, 91%	[87]
$\text{Pd}_1\text{O}_4/\text{ZSM-5}$	incipient wetness impregnation	$\text{Pd}(\text{NO}_3)_2$	0.01 wt% Pd	MFI	H_2O_2	95	HCOOH, 323	HCOOH, 78%	[11]
IrFe/ZSM-5	wet impregnation	$\text{H}_2\text{IrCl}_6 \cdot 6\text{H}_2\text{O}$ $\text{FeCl}_3 \cdot 6\text{H}_2\text{O}$	0.01 wt% Ir 0.6 wt% Fe	MFI	H_2O_2	50	HCOOH, 182	HCOOH, 71%	[88]
Au/ZSM-5	deposition-precipitation	$\text{HAuCl}_4 \cdot 3\text{H}_2\text{O}$	0.5 wt% Au	MFI	O_2	240	CH_3COOH , 13	CH_3COOH , 71%	[89]
Rh/Na-ZSM-5	incipient wetness impregnation	$\text{Rh}(\text{NO}_3)_3$	0.5 wt% Rh	MFI	O_2	150	CH_3COOH , 2200	CH_3COOH , 90%	[14]
Rh/ZSM-5	incipient wetness impregnation	$\text{Rh}(\text{NO}_3)_3$	0.1 wt% Rh	MFI	O_2	150	CH_3COOH , 820	CH_3COOH , 70%	[13]
Fe/ZSM-5	wet impregnation	$\text{FeCl}_3 \cdot 6\text{H}_2\text{O}$	0.31 wt% Fe	MFI	H_2O_2	50	CH_3COOH , 925	CH_3COOH , 100%	[90]

Methane selective oxidation to methanol is an important pathway for the direct exploitation of remote natural gas [66]. However, methanol is more easily oxidized to carbon dioxide than methane. Zeolites exhibit good catalytic activities and excellent shape selectivity in the catalytic oxidation. Metal-exchanged zeolites are believed to be effective in the selective oxidation of methane to methanol. Pioneering work on the use of metallozeolites for the selective oxidation of methane was conducted by Panov's group in the 1990s. They reported the formation of highly active oxygen species (named α -oxygen) by carrying out the oxygen isotope experiments to prove the irreversible binding of CO and CH_4 [91–94]. Such metal-exchanged zeolitic catalysts can selectively induce the breakage of C–H bonds in methane, and prevent methanol from excessive oxidation to generate other by-products [10]. In the last century, the most widely studied catalysts are molybdenum oxide, vanadium oxide, and iron compounds. In the 21st century, however, the research focus has turned to the iron- and copper-containing zeolites [10]. Some authors have reported the preparation of the Fe-, Cu-, and Ni-exchanged zeolites via an ion exchange route. These metal-exchanged zeolites exhibited excellent stability and selectivity in the partial oxidation of methane [66,67,95].

The following content will focus on the application of ion-exchanged zeolites in the selective oxidation of methane to methanol, in which methanol selectivity was closely related to the structure of the active metals in zeolites (e.g., monomers, oligomers, or metal oxide nanoparticles). Yu and coworkers [68] reported that, through a series of characterization studies on, it is proved that the mononuclear Fe^{3+} species stabilized outside the ZSM-5 framework was the active site of methane oxidation over the Fe/ZSM-

5 catalysts, as confirmed by the ^1H and ^{13}C NMR (nuclear magnetic resonance) results. Yu et al. [96] also used three different methods (i.e., incipient wetness impregnation, liquid ion-exchange, and solid-state ion-exchange) to obtain the Fe/ZSM-5 catalysts, and found that, through scanning electron microscopy (SEM), ultraviolet–visible spectroscopy (UV–Vis), and ^{57}Fe Mössbauer spectroscopy, the Fe-ZSM-5 catalyst synthesized through the solid-state ion-exchange approach possessed the highest proportion (71%) of the monomer Fe species. In addition, the catalyst derived from the solid-state ion-exchange route showed the highest yield and selectivity, which directly proved the role of the monomeric Fe species. Tabor et al. [69] pointed out that the stable binuclear Fe^{2+} active substance in the Fe-ferrierite zeolite catalyst possessed the ability to induce oxygen cracking at room temperature. The α -oxygen $[(\text{Fe}(\text{IV})=\text{O})]^{2+}$ exhibited the unique performance in the oxidation of methane to methanol at room temperature (methanol selectivity = 93%). The authors also found that the Fe(II)/Fe(IV) redox cycle could be repeated, which provided a prospect for the development of the highly active and stable methane-oxidation-to-methanol system.

In order to explore the role of different precursors in the catalyst, Kim and coworkers [70] prepared the Fe-ZSM-5 catalysts by the incipient wetness impregnation and ion-exchange methods with FeSO_4 , FeCl_2 , $\text{Fe}(\text{CH}_3\text{CO}_2)_2$, $\text{Fe}_2(\text{SO}_4)_3$, FeCl_3 , and $\text{Fe}(\text{NO}_3)_3$ as Fe precursors. According to the activity evaluation data, it was found that the Fe-ZSM-5 catalyst prepared by the ion exchange method showed a higher activity and a higher selectivity, and that derived with FeCl_2 as a precursor performed the best. Combined with the UV-Vis spectroscopic and NO-FTIR (Fourier transform infrared spectroscopic) characterization results, the authors thought that the active sites of the catalyst were mainly the Fe^{2+} species outside the framework. Due to the high consumption of H_2O_2 during the selective oxidation of methane to methanol over the Fe-ZSM-5 catalyst, Sun and coworkers [71] observed that the lanthanum-modified (LaFe-ZSM-5) catalysts could enhance the selective oxidation of methane, and inhibit the consumption of H_2O_2 (methanol selectivity reached 99% at 50 °C). According to the in situ pyridine-FTIR results, they found that the introduction of La could reduce acidity of the Brønsted acid sites, thereby inhibiting the decomposition of H_2O_2 during methane oxidation. This study may provide a strategy for direct methane oxidation to produce valuable hydrocarbon products, and further improve the catalyst to increase H_2O_2 consumption. In addition, the loading amount of Fe could also influence its state present in ZSM-5. Bell and coworkers [70] found that, when the Fe/Al ratio ≤ 0.56 , the FeO_x small particles tended to be formed; when the Fe/Al ratio ≤ 0.19 , most Fe existed in the form of Fe^{3+} (which was present in $[\text{Fe}(\text{OH})_2]^+$). Li et al. [79] also used DFT calculations to substantiate that the monomer Fe^{2+} species was preferentially stable in the SSZ-13 zeolite, and its oxidation activity of proximal Al to some CH_4 was higher than that over the catalyst with the dimer Fe^{2+} species.

Similarly, the pore size of zeolite also influenced selectivity and activity of the reaction. Among the small cage zeolites (e.g., BEA, CHA, FER, and MOR), the selectivity of Fe species to methanol was better. Although the chabazite and zeolite beta had the same chemical environment of the Fe species, they showed different activities for methane oxidation [97,98]. By regulating the fine structure of molecular sieve cage, Solomon et al. [99] explored the role of molecular sieve cage in methane oxidation. They employed the BEA and CHA zeolites with similar compositions, and used Mössbauer spectroscopy to track the change form of the Fe active sites during the primary conversion of methane. After analyzing the coordination environment of the Fe in Mössbauer spectra, it can be found that the state of α -Fe(IV)=O in the two zeolites was very different (Figure 2A). In the Mössbauer spectrum of Fe in the methane atmosphere, 80% of α -Fe(IV)=O was converted into the Fe(III) component, and another 17% of Fe was present in the form of α -Fe(III)–OH. In addition, resonance Raman spectroscopy further proved that, after reaction with methane, α -Fe(IV)=O was converted to the inactive α -Fe(III)–OH and α -Fe(III)–OCH₃. For the CHA zeolite, the amounts of the inactive α -Fe(III)–OH and α -Fe(III)–OCH₃ were very low (Figure 2B). These researchers further studied the influence of pore size of the molecular sieve on the CH_4 or CH_3^* diffusion using the theoretical calculations. The theoretical simulation results

showed that, for the BEA zeolite, the external diffusion of CH_3^* was barrier-free, which was conducive to the interaction between CH_3^* radicals and $\alpha\text{-Fe(IV)=O}$ combination to produce the inactive $\alpha\text{-Fe(III)-OCH}_3$ and $\alpha\text{-Fe(III)-OH}$. For the CHA zeolite, the energy barrier of CH_3^* radical diffusion was 5.2 kcal/mol. The experimental results revealed that the pore size of the molecular sieve was the key to determine the catalytic activity, which controlled the active species by affecting the diffusion of CH_3 free radicals ($\alpha\text{-Fe(IV)=O}$) of deactivation (Figure 2C).

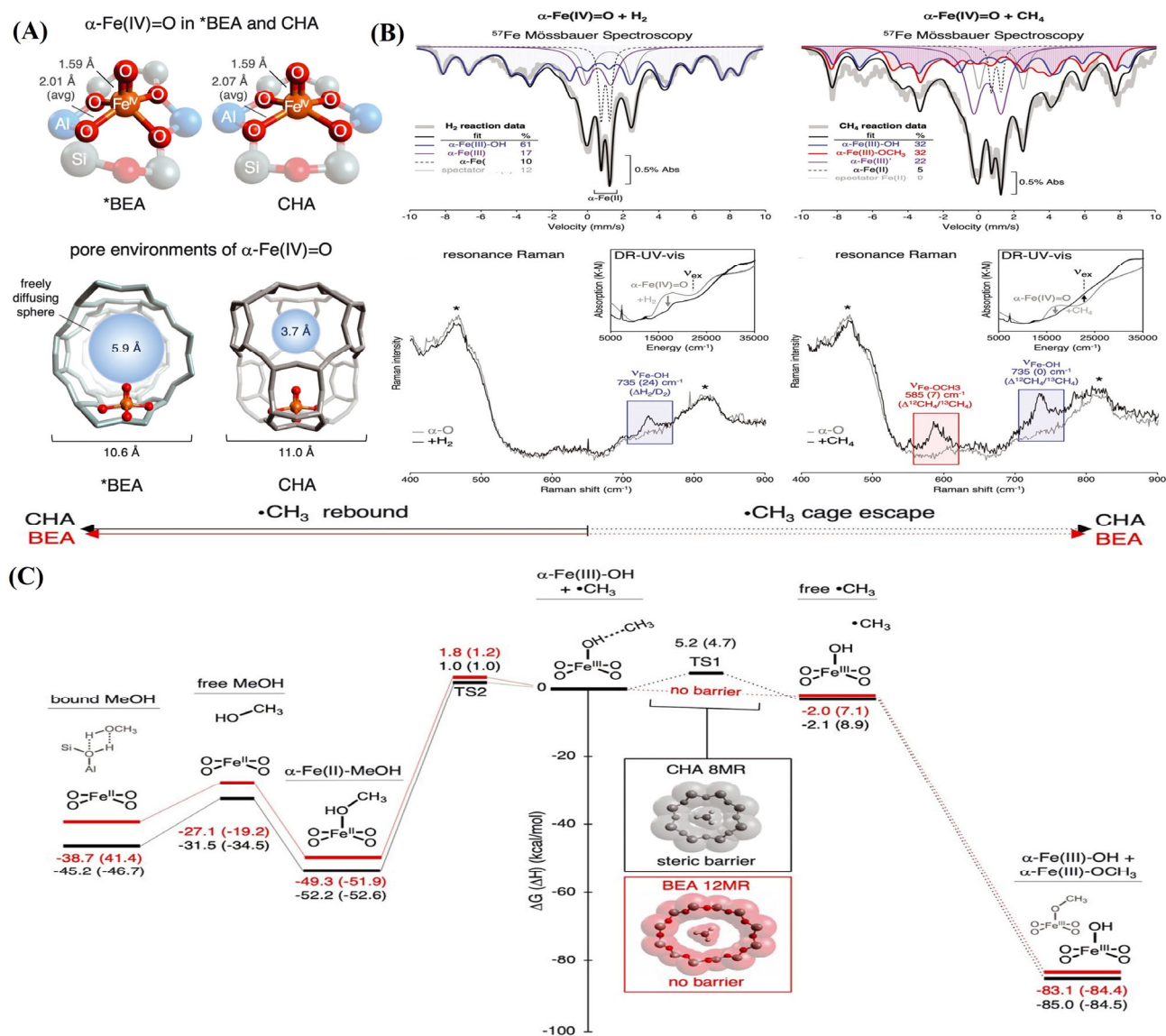


Figure 2. (A) Local environments of $\alpha\text{-Fe(IV)=O}$ sites in *BEA and CHA; (B) identification of Fe(III) species after H_2 and CH_4 reactions with Fe-*BEA; and (C) comparison of reaction coordinates for *BEA (red) and CHA (black) after H-atom abstraction. Reprinted/adapted with permission from Ref. [72]. Copyright 2021, copyright American Association for the Advancement of Science.

In addition to the Fe-zeolite catalysts, the Cu-zeolite catalysts also show good catalytic performance for such reactions. Copper species could also prevent the excessive oxidation of methane, and methanol was its main oxidation product [28]. Similar to the Fe-containing zeolites, copper in zeolites could be present in monomeric and dimeric forms. Unlike Fe-zeolites, Cu species underwent a $\text{Cu}^{\text{II}}/\text{Cu}^{\text{I}}$ cycle during the methane oxidation process. However, some authors also proposed the formation of $\text{Cu}^{\text{III}}=\text{O}$ [99]. Yoshizawa et al. [100]

calculated partial oxidation of methane of $[\text{Cu}_2(\mu\text{-O})]^{2+}$ and $[\text{Cu}_3(\mu\text{-O})_3]^{2+}$ on the MOR and MAZ cycle systems. The two aluminum anti-positions in the MOR zeolite formed two different $[\text{Cu}_2(\mu\text{-O})]^{2+}$ structures that could crack the C–H bonds in methane. The calculation results further showed that the addition of water molecules helped to reduce the desorption energy of methanol, and two of the bridged O atoms in $[\text{Cu}_3(\mu\text{-O})_3]^{2+}$ –MOR and $[\text{Cu}_3(\mu\text{-O})_3]^{2+}$ –MAZ displayed significantly different reactivities to methane. In addition, Li et al. [101] carried out the DFT calculations, and verified that the $[\text{Cu}_3(\mu\text{-O})_3]^{2+}$ species was more stable than the $[\text{Cu}_2(\mu\text{-O})]^{2+}$ species in ZSM-5. The Cu-oxo cluster in $[\text{Cu}_3(\mu\text{-O})_3]^{2+}$ was more conducive to the direct conversion of methane to methanol.

However, the real catalytic centers were still highly debatable. Heyer et al. [102] used the UV–Vis, (electron paramagnetic resonance) EPR, and XAS techniques to demonstrate that the reactivity of the binuclear $[\text{Cu}_2\text{O}]^{2+}$ site was significantly higher than that of the mononuclear $[\text{CuOH}]^+$ site. Sushkevich et al. [103] confirmed that Cu–O–Cu in Cu-MOR was the activity site of methane oxidation to methanol. Dinh et al. [73] used in situ XAS spectroscopy to verify that the $[\text{Cu–O–Cu}]^{2+}$ species was formed in the SSZ-13 zeolite cage via proton-assisted hydration of the Cu ions, which was the main active sites for the selective oxidation of methane. They also found that the selectivity to methanol was 98% at 270 °C. In a recent study, however, monomer copper was also found to be highly active and selective for methane oxidation. Yang and coworkers [74] reported a Cu-CHA catalyst, which exhibited an outstanding methanol space-time yield of 543 mmol/(mol_{Cu} h) with a selectivity of up to 91%. In order to explore the impact of zeolite structure on Cu species, Bokhoven and coworkers prepared a series of the Cu ion-exchange zeolite frameworks (e.g., MOR, EON, MAZ, MEI, BPH, FAU, LTL, MFI, HEU, FER, SZR, and CHA) [75].

It was found that selecting the appropriate zeolite-anchoring metal active sites could obtain a higher methanol yield, and the MAZ-type zeolite showed the highest yield, in which a number of the copper-oxo active species in the 8-membered ring channel of zeolite were formed. A higher copper-oxo reduction temperature led to a lower yield of methanol, whereas a lower copper-oxo reduction temperature gave rise to a lower selectivity of methanol. In addition, the authors also found that small pore zeolites exhibited good restrictions on the types of methane and metals, so it could efficiently catalyze methane oxidation to methanol at low reaction temperatures. Other researchers also obtained the same results [104,105]. The 8-membered ring in mordenite not only enhanced the activity of clusters, but also provided a closed environment for the highly selective and stable methane oxidation [76]. Working on the impact of the co-cation (H^+ and Na^+) in the Cu-MOR and Cu-ZSM-5 catalysts on the morphology of Cu and the activity of the catalyst in the cyclic reaction of methane to methanol, Davis and coworkers [67] pointed out that the active site structure of the catalyst depended upon the co-cation. The H-type zeolite contained a high concentration of the mono- μ -oxo dicopper(II) species, which was more selective for methanol generation. However, the Na-type zeolite contained a high concentration of the μ -1,2-peroxo dicopper(II) species, which facilitated methane oxidation to other products. The results of DFT calculations revealed that the mono- μ -oxo dicopper(II) species was preferentially formed in the 8-membered ring. As Na and Cu competed for the ion exchange sites, however, part of Cu was replaced in the 12-membered ring, thus influencing the morphology of Cu and the selectivity of the catalyst. In order to further clarify the impact of the small cage zeolite on methanol selectivity, Studt and coworkers [106] conducted the DFT calculations and found that three possible Cu species ($[\text{CuOO}]^+$, $[\text{CuO}]^+$, and $[\text{CuOH}]^+$) were identified, and the $[\text{CuOH}]^+$ species in the 8-membered ring was the main active site in the Cu-SSZ-13 catalyst, the 6-membered ring was not conducive to the reaction, while the 8-membered ring was conducive to the formation of the active $[\text{CuOH}]^+$ species. Suskevich et al. [107] also confirmed that a higher Si/Al ratio favored the improvement in methanol selectivity. CH_4 -TPD (temperature-programmed desorption) and in situ X-ray absorption near edge structure (XANES) results showed that the reactivity of the monomer Cu species to methane was low.

In addition, the methane anaerobic oxidation gave rise to the generation of hydrogen, while the copper monomer sample was only active under the O₂ conditions. DFT calculations indicated the similar steps of methane activation in monomer and dimer, but the stability of methoxy group in monomer was better. In order to significantly explore the influence of element composition on productivity and Cu morphology, Pappas and coworkers [77] prepared the Cu-SSZ-13 zeolites, and investigated the linear relationship between the reducibility of the zeolitic material and methanol productivity. It was shown that the tri-coordinated Cu^{II} centers (with two O_{fw} and one O_{ef} ligands in the metal coordination sphere) were the most favorable sites for methane conversion. A high-temperature treatment increased formation of the tri-coordinated Cu^{II} species, while at low temperatures, the four-coordination Cu^{II} species were more conducive, leading the catalysts to show a low methanol productivity. These authors also found that the XAS measurements clearly evidenced a positive linear correlation between methanol productivity and Cu centers reducibility. Under the condition of low Si/Al ratios and low Cu loadings, the conversion of methane to methanol was poor. However, the catalysts with the Si/Al ratios of 12–15 and a Cu loading of 0.5 exhibited the highest methanol yields, which was 0.2 mol CH₃OH/mol Cu (i.e., 125 mmol_{CH₃OH}/g_{Cu}).

Since the reaction mechanism of methane selective oxidation to methanol is complex, we herein briefly introduce the reaction mechanisms of methane oxidation over the iron- and copper-containing zeolite catalysts. Pidko and coworkers [78] performed the DFT calculations to investigate the mechanism of methane oxidation in the presence of H₂O₂ at the defined Fe sites in the Fe/ZSM-5 zeolite. [(H₂O)₂-Fe(III)-(μO)₂-Fe(III)-(H₂O)₂]²⁺ was used as a model, and H₂O₂ was used to activate this cluster to form the Fe(III)-oxo and Fe(IV)-oxo complexes that could dissociate methane. As shown in Figure 3A, these active sites promote the cracking of C–H bonds in methane according to three ways. The Fe(III)-oxo complex catalyzes the heterolytic and Fenton-type reactions, while the Fe(IV)-oxo complex promotes the homolytic oxidation of methane. The C–H bond activation step is followed by the formation of MeOH and MeOOH, and the regeneration of the active site. By further calculation, the authors found that methanol could be formed by the recombination of CH₃– and OH– radicals to activate the C–H bonds. If the C–H bond was previously heterolytically reacted, this step could either precede or follow the oxidation of the active site via the peroxy bond cleavage.

As shown in Figure 3B, Chen et al. [108] explored the direct oxidation pathways of methane to methanol at the binuclear Fe site, and realized that H₂O could be used as an active site regulator, which induced the transformation of the binuclear Fe site ([Fe–O–Fe]²⁺ → [FeOH]⁺–[FeOH]⁺ → [FeOH]²⁺–O–[FeOH]²⁺). It could easily react with the generated CH₃– and OH– radicals to generate CH₃OH and regenerate H₂O, which was related to the generation of the [Fe–O–Fe]²⁺ species in the next cycle. At the same time, the [FeOH]²⁺–O–[FeOH]²⁺ sites could also effectively inhibit the peroxidation of CH₃OH and carbon deposition, and then effectively promote methanol production.

Bokhoven et al. [104] believed that there were two reaction mechanisms of methane oxidation over the Cu-zeolite catalysts: one was that the electrons required for methane oxidation existed at the oxygen atom in the active site in the form of oxygen radicals, thus oxidizing methane to methanol; the other was that copper in the catalysts was reduced from Cu(II) to Cu(I), which affected the conversion of methane to methanol. Studt et al. [106] explored the methane dissociation at the [CuOH]⁺ site in the CHA zeolite, and found that the insertion of CH₃– radicals into the oxygen atom of the [CuOH]⁺ site was energetically unfeasible. In contrast, the addition of CH₃– radicals to the Cu atom to form a [Cu–H₂O–CH₃]⁺ species attached to the CHA framework (Figure 4A) was easier. When water was introduced into this reaction system, the freely diffusible [Cu–2(H₂O)–CH₃]⁺ species were released from the framework. Therefore, there were two routes for methanol production: one was the self-decomposition to methanol, and the other was the migration of one H atom from the solvated species to the zeolite framework and methanol was finally formed.

Alayon and his or her colleagues studied the reduction and oxidation of copper ions in Cu-MOR, and observed the change in the valence state of the copper species caused by methane activation (Figure 4B) [79]. For the Cu-MOR catalyst after high-temperature dehydration and oxygen activation, Cu^{2+} was converted into the mono- μ -oxo dicopper(II) species. In the reaction with methane, (i) about half of the Cu^{II} sites were reduced to the Cu^{I} species, and a small part of the Cu^{II} species was bound with water or OH^- radicals; and (ii) the CH_3^- radicals combined with the mono- μ -oxo dicopper(II) species to form the $[\text{Cu}^{\text{I}}-\text{OCH}_3-\text{Cu}^{\text{II}}]$ species, which could promote methanol desorption. In addition, the water-stable Cu^{II} oxide species were also able to oxidize methane to methanol, indicating that the redox reaction existed in the oxidation process of methane to methanol. Most reports have discussed the redox mechanisms of methane oxidation over the catalysts with the conversion of Cu(II) to Cu(I). Adeyiga and coworkers explored the $[\text{Cu}_3(\mu\text{-O})_3]^{2+}$ electronic structure and function in methane activation (Figure 4C) [109]. Cu mainly existed in the form of Cu^{II} . According to the electronic energy analysis of C–H bonds, the activity of the O(1) site was higher than that of the O(2) or O(3) site. Methane was cleaved and activated by the homogenous C–H bonds at the O(1) site to generate the gas phase CH_3^- radicals, and the OH^- groups were bound with the $[\text{Cu}_3(\mu\text{-O})_3]^{2+}$ active sites. Then, the CH_3^- radicals were transformed to the OCH_3 species at the active site. Finally, CH_3OH and H_2 were released by adding water. Although the above theoretical work shows several feasible pathways of methane oxidation, there are still some uncertainties due to the difficulty in capturing reaction intermediates.

In this part, we have explored the structure of the active metals in zeolites and pore sizes and acidity of zeolites, which can influence the activity and selectivity of Fe- and Cu-zeolite catalysts. In zeolites with different structures, the active metals show different coordination environments, thus exhibiting different catalytic activities and selectivities. There are some difficulties in exploring the reaction mechanisms. In conclusion, the synthesis of zeolite-based catalysts with stable cooperative interaction between metal centers and supports that offers a better control of the coordination environment is the key challenge that needs to be dealt with in the future.

2.3.2. Selective Oxidation of Methane to Formaldehyde

Formaldehyde is another product of methane selective oxidation, as can be seen from the works carried out by many researchers. Beznis et al. [39] explored the effects of acid and alkali treatments on the product selectivity of the Co-ZSM-5 zeolitic catalysts. It was found that the zeolite external surface area increased after the alkali treatment, and then accommodated more amounts of the Co_3O_4 and CoO species, which were more selective to methanol formation. After the acid treatment, the amount of the highly dispersed Co^{2+} species in the zeolite channels increased, hence rendering to achieve a higher selectivity to formaldehyde (75%). Lucas et al. [110] reported that the Mo/ZSM-5 catalyst treated with ammonia showed a high formaldehyde selectivity (73%), which was due to the specificity of the monomer $\text{Mo}=\text{O}$ site in the treated catalyst for formaldehyde production. In addition, zeolite-supported metal oxide clusters were also used for the selective oxidation of methane to formaldehyde. However, mesoporous SBA-15 and MCM-41 materials have also attracted extensive attention in recent years. For example, the supported ferric phosphate catalyst showed good activity in the selective oxidation of methane to oxygenates [80,81]. Wang et al. [82] investigated methane conversion and formaldehyde selectivity over the 20–40 wt% $\text{FePO}_4/\text{MCM-41}$ catalysts, and found that, when the FePO_4 loading was lower than 40 wt%, the ferric phosphate clusters were highly dispersed on the surface of mesoporous MCM-41; while, when the FePO_4 loading was higher, the crystalline phase of ferric phosphate was mainly tridymite phase. At 300–500 °C, the main products of methane oxidation were methanol, formaldehyde, and dimethyl ether, while formaldehyde was mainly formed together with carbon oxides at relatively high temperatures (The selectivity to formaldehyde was 79%). In order to explore the activity of ferric phosphate supported on different supports for the production of formaldehyde from methane oxidation, Wang et al. [83]

found that the forms of iron phosphate in the $\text{FePO}_4/\text{SBA-15}$ and $\text{FePO}_4/\text{MCM-41}$ catalysts were similar, the $\text{FePO}_4/\text{SBA-15}$ catalysts showed better redox performance and larger pore sizes as compared with the $\text{FePO}_4/\text{MCM-41}$ catalysts, thus the former exhibiting better catalytic activity and selectivity than the latter, and furthermore 5 wt% $\text{FePO}_4/\text{SBA-15}$ gave the highest formaldehyde selectivity (81%). In addition, proper acidity helps to stabilize methanol products and prevent their continuous overoxidation. The $\text{VO}_x/\text{SBA-15}$ and $\text{VO}_x/\text{MCM-41}$ catalysts with a good dispersion of VO_x species showed a high turnover frequency (TOF) of 0.48 for formaldehyde formation [84,85]. Wang et al. [86] claimed that, when the copper content was 0.008 wt% and the Si/Cu ratio was 13200, the $\text{CuO}_x/\text{SBA-15}$ catalyst performed the best, and the specific site rate for formaldehyde formation was 5.6 mol/(mol_{Cu} s). The EPR characterization results demonstrated that the Cu^{I} sites produced during the reaction process could enable O_2 molecules to form the active oxygen species, which then selectively oxidize methane to formaldehyde.

In order to explore the reaction mechanism of the selective oxidation of methane to formaldehyde, Wang et al. [87] employed the pulse reaction and EPR techniques to explore the reactivity of the lattice oxygen in $\text{CuO}_x/\text{SBA-15}$ or the oxygen species related to the Cu sites. As shown in Figure 5A, methane could react with the lattice oxygen on the catalyst surface to generate CO and CO_2 , and at the same time, part of the Cu^{II} sites could be reduced to Cu^{I} by methane. The rise in Cu^{I} concentration at the initial reaction stage increased both methane conversion and formaldehyde selectivity. Hence, the Cu(I) site generated under the reaction conditions accounted for the activation of O_2 to provide an active oxygen species for the selective oxidation of methane to formaldehyde.

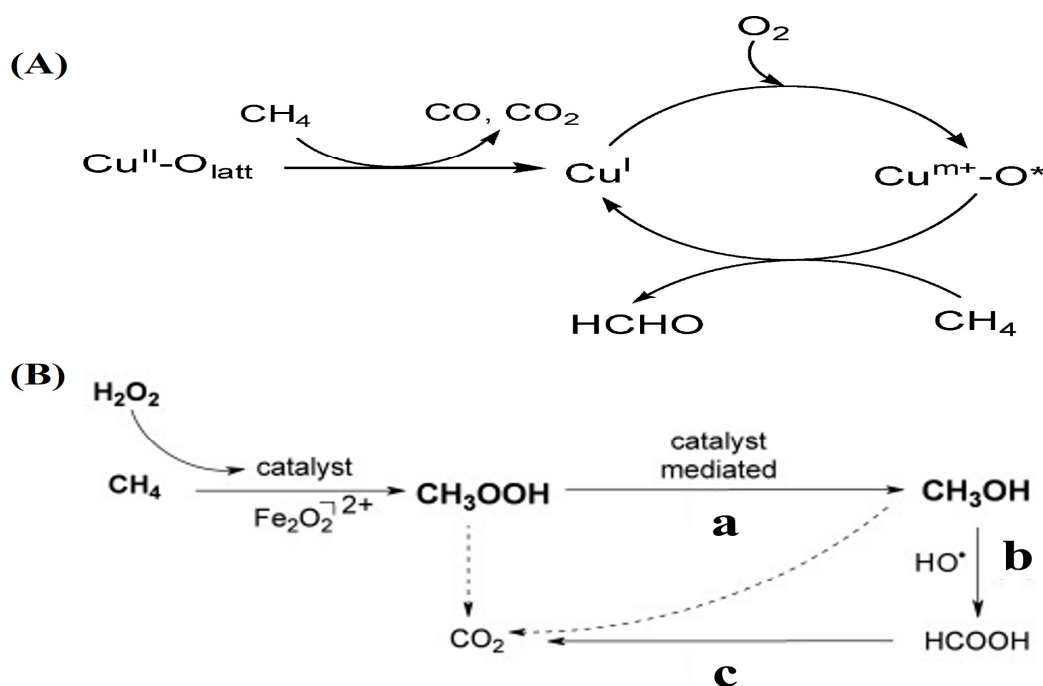


Figure 5. (A) Reaction mechanism for the selective oxidation of CH_4 to HCHO over the $\text{CuO}_x/\text{SBA-15}$ catalyst. Reprinted/adapted with permission from Ref. [87]. Copyright 2008, copyright American Chemical Society, and (B) proposed reaction networks for the oxidation of methane over ZSM-5(30). Reprinted/adapted with permission from Ref. [111]. Copyright 2012, copyright Willy-VCH GmbH.

In summary, we have briefly analyzed the research works on the selective oxidation of methane to formaldehyde by molecular sieves and porous materials. However, it also faces many challenges, such as the control of catalyst life, selectivity and yield of formaldehyde, and reaction temperature and pressure. Therefore, the future research direction should focus on improving catalytic performance and stability of the catalyst, further understanding the reaction mechanisms, and optimizing the reaction conditions.

2.3.3. Selective Oxidation of Methane to Formic Acid

In addition to methanol and formaldehyde, formic acid is also one product of the selective oxidation of methane. The Fe-containing zeolite has been recognized as a potential catalyst for the selective oxidation of methane. Yang et al. [112] used the ball-milling method to transform the isolated Fe^{3+} in Fe/ZSM-5 to the highly active Fe species outside the skeleton. After ball milling, the 0.03 wt% Fe/ZSM-5 catalyst showed high activity (formic acid selectivity = 96% at 70 °C) and good stability. Zhu and coworkers [88] prepared the Fe/ZSM-5 catalysts to investigate the selective conversion of methane to formic acid. Over the Fe/ZSM-5 catalyst for this reaction, the HCOOH yield was 383.2 mmol/(g_{cat} h), and the TOF was the highest (at a space velocity of 84,200 h⁻¹) among all of the previously reported zeolite- and noble metal-based catalysts. The results of EPR characterization and DFT calculations revealed that the Fe–O active site confined by ZSM-5 could easily dissociate the C–H bonds by the radicals under mild conditions, and then the O radicals oxidized HCHO to HCOOH at the Fe–O active site.

Methanol was considered as the intermediate product of further oxidation to formic acid [89]. As shown in Figure 5B, in the presence of hydrogen peroxide and a catalyst, the reaction with methane generates the main intermediate product CH₃OOH. CH₃OOH may be further decomposed or react to form CH₃OH, and then CH₃OH and –OH radicals react to form formic acid [111]. In addition, Yu et al. [68] found that the adjacent Brønsted acid sites of ZSM-5 were conducive to the activation of methane, and methane was first oxidized to CH₃OOH and CH₃OH, which were then converted into HOCH₂OOH and finally into formic acid. Shahami and coworkers [113] also reported that the presence of strong acidity was favorable for the formation of formic acid instead of methanol. Over the Fe–Cu–ZSM-5 catalysts for the selective oxidation of methane, however, Hammond and coworkers [114] claimed that the Cu²⁺ species could promote the formation of methanol and inhibit the excessive oxidation of other oxygenates by methanol. Dinh et al. [71] believed that the Cu species controlled the population of –OH radicals impeding the further oxidation of methanol to formic acid.

In addition to transition metals, noble metals are also used for the selective oxidation of methane. Tao et al. [115] prepared the Pd₁O₄/ZSM-5 single-atom catalyst for methane oxidation. As shown in Figure 6A, the increase in loading exerted little effects on the yield of methane selective oxidation to other oxygenates, the 0.01 wt% Pd/ZSM-5 catalyst showed the highest total yield of formic acid, methyl peroxide, methanol, and CO₂, with formic acid selectivity being the highest (78%). The authors also found that the introduction of CuO species significantly enhanced methanol selectivity and inhibited the generation of other oxygenates (Figure 6B). Yu et al. [11] studied the selective oxidation of methane over the IrFe/ZSM-5 catalysts, and found that 0.1Ir–0.6Fe/ZSM-5 exhibited a high oxygenates yield of 3192 μmol/(g h) at 50 °C, which was three times higher than that over Fe/ZSM-5. The selectivity of formic acid increased from 54 to 71.3%. X-ray absorption fine structure (XAFS) characterization showed that the introduction of Ir led to the formation of the Ir–O–Fe structure in the Fe/ZSM-5 catalyst, promoted the activation of C–H bonds, and improved the utilization of H₂O₂.

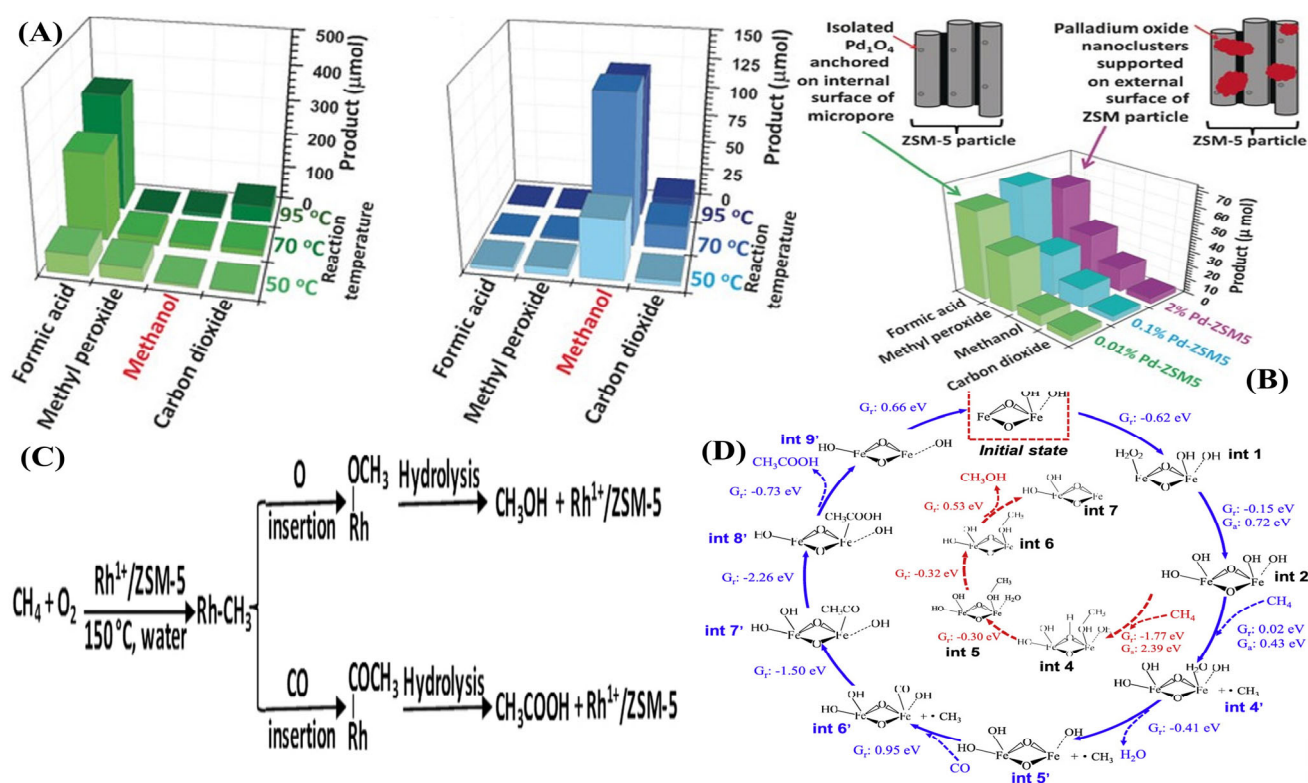


Figure 6. (A) Yields of products of transformation of CH₄ catalyzed by 0.01, 0.10, and 2.0 wt% Pd/ZSM-5 for methane partial oxidation at 50 °C; (B) catalytic performance of 0.01 wt% Pd/ZSM-5 at 50, 70, and 95 °C, and 0.01 wt% Pd/ZSM-5 loaded with 2 wt% CuO at 50, 70, and 95 °C, the plotted yields of products formed over 28 mg 0.01 wt% Pd/ZSM-5, or 0.01 wt% Pd/ZSM-5 loaded with 2.0 wt% CuO were the values after subtraction of the yields of the products formed over 28 mg of ZSM-5 (without the Pd sites) under the same catalytic conditions. Reprinted/adapted with permission from Ref. [115]. Copyright 2016, copyright Willy-VCH GmbH, (C) the conversion to methanol and acetic acid followed independent reaction pathways. Reprinted/adapted with permission from Ref. [14]. Copyright 2017, copyright Springer Nature Ltd., and (D) proposed reaction networks for the CH₃OH/CH₃COOH formation, the calculated Gibbs reaction energy, as well as the free energy barriers. Reprinted/adapted with permission from Ref. [116]. Copyright 2022, copyright Elsevier Ltd.

In this section, we have carried out a simple analysis on the noble-metal and transition-metal zeolite catalysts for the selective oxidation of methane to formic acid. Compared with the selective oxidation of methane to formaldehyde, the selective oxidation of methane to formic acid is more abundant in reactants and more diversified in reaction products. Therefore, how to control the side reactions and the production of other products is the key issue in the selective oxidation of methane to formic acid.

2.3.4. Selective Oxidation of Methane to Acetic Acid

Acetic acid is an important intermediate in the production of high-value chemicals. As we all know, methane can be oxidized to generate not only carbon monoxide, carbon dioxide, methanol, formaldehyde, and formic acid, but also acetic acid. Recently, Qi et al. [90] have proven that the Au/ZSM-5 catalysts could selectively convert methane to methanol and acetic acid under the condition of only oxygen, which also did not need a reducing agent. However, the real active centers and appropriate oxidants choices need to be further investigated. Preliminary studies showed that CO insertion could form the stable Rh-carbonyl species, which possessed a high activity for methane carbonylation to acetic acid. Shan et al. [14] reported that the Rh single-atom catalyst could effectively catalyze the direct conversion of methane to methanol or acetic acid (The selectivity to

acetic acid achieved 90%) through changing the acid sites of the zeolite. It was found that the Rh@Na-ZSM-5 catalyst containing a small amount of the Brønsted acid sites could make methane selectively be converted to methanol, while methane oxidation over the Rh@HZSM-5 catalysts with a more amount of the Brønsted acid sites could directionally generate acetic acid. The authors conducted the DFT calculations and isotope-labeling measurements to explore the reaction pathways of the direct conversion of methane to oxygenates (Figure 6C). First, methane forms the Rh-CH₃ species after the interaction of oxygen, water, and the catalyst, then the Rh-CH₃ species were further transformed to the Rh-OCH₃ species through the insertion of oxygen, or the Rh-COCH₃ species were formed through the CO insertion reaction, which were finally hydrolyzed to produce methanol and acetic acid, respectively.

Yu et al. [13] also prepared the Rh/ZSM-5 single-atom catalyst for the selective oxidation of methane. The results showed that the Rh₁O₅ site anchored in the zeolite exhibited the best catalytic activity, and the selectivity to acetic acid reached 70%, which was 1000 times higher than that of the free Rh³⁺ in the aqueous solution. Isotopic studies demonstrated that acetic acid was not formed by the carbonylation of methanol with carbon monoxide, which was the same as that reported by Shan and coworkers. Wang et al. through immobilizing the Ir complex on oxide support to realizes carbonylation of oxidized methane [116]. The experimental results show that the catalyst prepared by this method can not only directly activate methane, but also easily separate and reuse the catalyst. In addition, they also found that the electrophilic sensitivity of methyl migration to carbonyl can be controlled by adjusting the valence of the Ir species. The as-prepared catalysts dominated by Ir (IV) were more likely to produce acetic acid, while catalysts dominated by Ir (III) were more likely to produce methanol. In addition, Narsimhan and coworkers [116] studied the reaction mechanism of methane oxidation to acetic acid over the copper-exchanged zeolitic catalysts. It was found that Cu-H-MOR was an oxidant during the formation of acetic acid. The oxygen atoms fixed in the Cu cluster of Cu-H-MOR oxidized methane to methoxy, and then the methoxy formed over Cu-H-MOR was carboxylated with CO to generate acetic acid. In the production of acetic acid, however, the activity over Cu-Na-MOR was much lower than that over Cu-H-MOR. Furthermore, the Cu/Al ratio in Cu-Na-MOR was an important factor determining the catalytic activity of acetic acid generation. It is worth noting that Cu-Na-MOR with Cu/Al > 0.36 does not show activity for the formation of acetic acid, while Cu-Na-MOR with Cu/Al ≤ 0.36 exhibits activity for acetic acid generation. However, the Cu/Al ratio exerted no effects on the catalytic activity of Cu-H-MOR for the formation of acetic acid. The authors also found that the Brønsted acid sites and Cu_xO_y sites in Cu-H-MOR played an important role in methane activation to generate methoxy and methoxycarbonylation, which finally promoted the formation of acetic acid.

Recently, Wu et al. [117] prepared the Fe/ZSM-5 catalysts with the binuclear Fe sites, which possessed the [Fe(III)-(μO)₂-Fe(III)-(OH)₂] active sites and 100% acetic acid selectivity. As shown in Figure 6D, theoretical studies revealed that H₂O₂ was changed to the adsorbed -OH species at the binuclear Fe site, and then the -OH species reacted with methane to generate the -CH₃ radicals. CO adsorption further generated the adsorbed -CO species, and then the -CH₃ species was coupled with the -CO/-OH species to obtain the adsorbed acetyl and acetic acid species. Finally, CH₃COOH was formed and the binuclear Fe sites were regenerated. However, Fang et al. [118] demonstrated that the monomeric species could form the -OH and -OOH species, resulting in the formation of acetic acid. In addition, Deng and coworkers [117] reported the generation of acetic acid on the surface of ZnZSM-5 in the presence of methane and carbon monoxide according to the results of the in situ ¹³C MAS (magic angle spin) NMR characterization. It was found that a small amount of O₂ promoted the formation of the Zn-CH₃ species, which was trapped by CO₂ to form acetic acid. The presence of H₂ was conducive to generation of the Zn-OCH₃ species, in which acetic acid was formed via the Koch-type mechanism. More importantly, the two reaction pathways are likely controllable by varying the redox conditions, which

provides a new perspective for the selective conversion of small alkanes and co-reactants to more valuable chemicals.

Although the selective oxidation of methane to acetic acid shows good sustainability and environmental friendliness. However, there are still some difficulties in the optimization of reaction conditions, the stability and activity of catalysts, and the selectivity and yield of products.

3. Conclusive Remarks and Perspectives

Recent studies have shown that zeolite-supported catalysts favor the oxidation of methane. In this review article, the properties of active sites, the role of pore limitation, the ability to activate C–H bonds, and the reaction mechanisms of different zeolites-supported catalysts for methane oxidation were discussed in detail, and applications of these materials in the complete and selective oxidation of methane were briefly introduced. The catalytic combustion of methane needs to be completed at high temperatures. At present, the conversion of methane to other valuable chemicals (e.g., methanol, formaldehyde, formic acid, acetic acid, and etc.) is the most attractive target in chemical industries. A number of studies have been carried out to open up new possibilities for establishing the relationship between specific active sites formed by two or three metal atoms in the zeolite-based catalysts. Although a lot of research works have been carried out in the past decades, upgrading methane-to-valuable chemicals via an efficient and sustainable route has not yet been realized.

In terms of the selective oxidation of methane, different by-products can be obtained due to different oxidation extents. Thus, preventing excessive oxidation of methane is also a challenging task. The size of metal species is a key factor governing activity of a catalyst. With the decrease in metal size, the amount of the active sites in the zeolite is increased, and the activity of the catalyst is hence enhanced. In recent years, single-atom catalysts have been regarded as a new star in heterogeneous catalysis due to their high atom utilization efficiency. However, there are few reports on the preparation and catalytic applications of zeolite-based single-atom catalysts, especially those with high thermal stability. From this point of view, it is urgent to develop the highly efficient zeolite-supported single-atom catalysts. In addition to supporting and binding effects of the zeolite skeleton, the inherent acid/base and redox properties of the zeolite can further promote activity of the metal species and enhance the catalytic performance. Moreover, the synergistic effect between zeolite and metal species is also considered as a strategy to improve the catalytic performance of methane oxidation. Due to the complex coordination environment of the metal species in the zeolite, however, it is difficult to obtain the working state of the active sites. Therefore, it is an important but challenging task to establish an analytical technique to clarify the actual catalysis mechanisms. In addition, it is also necessary to effectively combine theoretical calculations with experimental results, establish the suitable active site models, and propose reasonable reaction pathways. Although there are some innovations in the synthesis of zeolite-based catalysts, it is still desirable to develop the simple synthesis strategies with low cost, low energy consumption, and low pollution. Furthermore, the excellent performance of many catalysts is often highly dependent on the nature of the metal active sites. How to improve the utilization of the metals, design the metal active sites, or use the nonmetallic substitutes to achieve high performance in the important catalytic reactions is the focus of the future research work. In recent years, zeolite-supported catalysts have greatly promoted the development of heterogeneous catalysis fields, which is of great significance in the industrial development. We hope that this review article can help researchers to investigate methane oxidation over the zeolite-supported catalysts.

Author Contributions: Conceptualization, H.D.; Methodology, H.D.; Software, W.F., X.W., H.L. and J.T.; Investigation, L.W.; Resources, H.D.; Data Curation, W.F., X.W., H.L. and J.T.; Writing—Original Draft Preparation, L.W.; Writing—Review and Editing, H.D.; Visualization, Y.L., J.D. and L.J.; Supervision, H.D.; Project Administration, H.D.; Funding Acquisition, H.D.; All authors have read and agreed to the published version of the manuscript.

Funding: This work was supported by the State’s Key Project of Research and Development Plan (2022YFB3504101), National Natural Science Foundation Committee of China—Liaoning Provincial People’s Government Joint Fund (U1908204), and Foundation on the Creative Research Team Construction Promotion Project of Beijing Municipal Institutions (IDHT20190503).

Data Availability Statement: Not applicable.

Conflicts of Interest: The authors declare no conflict of interest.

References

1. Peng, H.; Rao, C.; Zhang, N.; Wang, X.; Liu, W.; Mao, W.; Han, L.; Zhang, P.; Dai, S. Confined ultrathin Pd-Ce nanowires with outstanding moisture and SO₂ tolerance in methane combustion. *Angew. Chem. Int. Ed.* **2018**, *57*, 8953. [[CrossRef](#)] [[PubMed](#)]
2. Saha, D.; Grappe, H.A.; Chakraborty, A.; Orkoulas, G. Postextraction separation, on-board storage, and catalytic conversion of methane in natural gas: A review. *Chem. Rev.* **2016**, *116*, 11436–11499. [[CrossRef](#)] [[PubMed](#)]
3. Zhu, W.L.; Shen, M.K.; Fan, G.Z.; Yang, A.; Meyer, J.R.; Ou, Y.N.; Yin, B.; Fortner, J.; Foston, M.; Li, Z.S.; et al. Facet-dependent enhancement in the activity of bismuth vanadate microcrystals for the photocatalytic conversion of methane to methanol. *ACS Appl. Nano Mater.* **2018**, *1*, 6683–6691. [[CrossRef](#)]
4. Choudhary, T.V.; Choudhary, V.R. Energy-efficient syngas production through catalytic oxy-methane reforming reactions. *Angew. Chem. Int. Ed.* **2008**, *47*, 1828–1847. [[CrossRef](#)] [[PubMed](#)]
5. Dai, Y.L.; Kumar, V.P.; Zhu, C.J.; Wang, H.Y.; Smith, K.J.; Wolf, M.O.; Maclachlan, M.J. Bowtie-shaped NiCo₂O₄ catalysts for low-temperature methane combustion. *Adv. Funct. Mater.* **2019**, *29*, 1807519. [[CrossRef](#)]
6. Thauer, R.K. Functionalization of methane in anaerobic microorganisms. *Angew. Chem. Int. Ed.* **2010**, *49*, 6712–6713. [[CrossRef](#)]
7. Olivos-Suarez, A.I.; Szecsenyi, A.; Hensen, E.J.M.; Ruiz-Martinez, J.; Pidko, E.A.; Gascon, J. Strategies for the direct catalytic valorization of methane using heterogeneous catalysis: Challenges and opportunities. *ACS Catal.* **2016**, *6*, 2965–2981. [[CrossRef](#)]
8. Han, J.Y.; Zemlyanov, D.Y.; Ribeiro, F.H. Catalytic combustion of methane on palladium single crystals. *Catal. Today* **2006**, *117*, 506–513. [[CrossRef](#)]
9. McCarty, J.G. Durable catalysts for cleaner air. *Nature* **2000**, *403*, 35–36. [[CrossRef](#)]
10. Ravi, M.; Sushkevich, V.L.; Knorpp, A.J.; Newton, M.A.; Palagin, D.; Pinar, A.B.; Ranocchiari, M.; Bokhoven, J.A.V. Misconceptions and challenges in methane-to-methanol over transition-metal-exchanged zeolites. *Nat. Catal.* **2019**, *2*, 485–494. [[CrossRef](#)]
11. Huang, W.; Zhang, S.; Tang, Y.; Li, Y.; Nguyen, L.; Li, Y.; Shan, J.; Xiao, D.; Gagne, R.; Frenkel, A.I.; et al. Low-temperature transformation of methane to methanol on Pd₁O₄ single sites anchored on the internal surface of microporous silicate. *Angew. Chem. Int. Ed.* **2016**, *55*, 13441. [[CrossRef](#)]
12. Zuo, H.L.; Meynen, V.; Klemm, E. Selective oxidation of methane with hydrogen peroxide towards formic acid in a micro fixed-bed reactor. *Chem. Ing. Tech.* **2017**, *89*, 1759–1765. [[CrossRef](#)]
13. Tang, Y.; Li, Y.T.; Fung, V.; Jiang, D.; Huang, W.X.; Zhang, S.; Lwasawa, Y.; Sakata, T.; Nguyen, L.; Zhang, X.Y.; et al. Single rhodium atoms anchored in micropores for efficient transformation of methane under mild conditions. *Nat. Commun.* **2018**, *9*, 1231. [[CrossRef](#)]
14. Shan, J.J.; Li, M.W.; Allard, L.F.; Lee, S.; Flytzani-Stephanopoulos, M. Mild oxidation of methane to methanol or acetic acid on supported isolated rhodium catalysts. *Nature* **2017**, *551*, 605–608. [[CrossRef](#)]
15. Shamzhy, M.; Opanasenko, M.; Concepcion, P.; Martinez, A. New trends in tailoring active sites in zeolite-based catalysts. *Chem. Soc. Rev.* **2019**, *48*, 1095–1149. [[CrossRef](#)]
16. Sun, Q.M.; Wang, N.; Yu, J.H. Advances in catalytic applications of zeolite-supported metal catalysts. *Adv. Mater.* **2021**, *33*, 2104442. [[CrossRef](#)]
17. Vogt, E.T.C.; Weckhuysen, B.M. Fluid catalytic cracking: Recent developments on the grand old lady of zeolite catalysis. *Chem. Soc. Rev.* **2015**, *44*, 7342–7370. [[CrossRef](#)]
18. Sudarsanam, P.; Peeters, E.; Makshina, E.V.; Parvulescu, V.I.; Sels, B.F. Advances in porous and nanoscale catalysts for viable biomass conversion. *Chem. Soc. Rev.* **2019**, *48*, 2366–2421. [[CrossRef](#)]
19. Dusselier, M.; Davis, M.E. Small-pore zeolites: Synthesis and catalysis. *Chem. Rev.* **2018**, *118*, 5265–5329. [[CrossRef](#)]
20. Sun, Q.; Xie, Z.K.; Yu, J.H. The state-of-the-art synthetic strategies for SAPO-34 zeolite catalysts in methanol-to-olefin conversion. *Natl. Sci. Rev.* **2018**, *5*, 542. [[CrossRef](#)]
21. Chen, L.H.; Sun, M.H.; Wang, Z.; Yang, W.M.; Xie, Z.K.; Su, B.L. Hierarchically structured zeolites: From design to application. *Chem. Rev.* **2020**, *120*, 11194–11294. [[CrossRef](#)] [[PubMed](#)]
22. Spivey, J.J.; Hutchings, G. Catalytic aromatization of methane. *Chem. Soc. Rev.* **2014**, *43*, 792–803. [[CrossRef](#)] [[PubMed](#)]

23. Vollmer, I.; Yarulina, I.; Kapteijn, F.; Gascon, J. Progress in developing a structure-activity relationship for the direct aromatization of methane. *ChemCatChem* **2019**, *11*, 39. [\[CrossRef\]](#)
24. Yang, L.; Huang, H.M. Transition-metal-catalyzed direct addition of unactivated C–H bonds to polar unsaturated bonds. *Chem. Rev.* **2015**, *115*, 3468–3517. [\[CrossRef\]](#)
25. Balcells, D.; Clot, E.; Eisenstein, O. C–H bond activation in transition metal species from a computational perspective. *Chem. Rev.* **2010**, *110*, 749–823. [\[CrossRef\]](#)
26. Schwach, P.; Pan, X.L.; Bao, X.H. Direct conversion of methane to value-added chemicals over heterogeneous catalysts: Challenges and prospects. *Chem. Rev.* **2017**, *117*, 8497–8520. [\[CrossRef\]](#)
27. Gunsalus, N.J.; Koppaka, A.; Park, S.H.; Bischof, S.M.; Hashiguchi, B.G.; Periana, R.A. Homogeneous functionalization of methane. *Chem. Rev.* **2017**, *117*, 8521–8573. [\[CrossRef\]](#)
28. Yang, S.Q.; Hu, T.L. Reverse-selective metal-organic framework materials for the efficient separation and purification of light hydrocarbons. *Coord. Chem. Rev.* **2022**, *468*, 214628. [\[CrossRef\]](#)
29. Kumar, P.; Al-Attas, T.A.; Hu, J.G.; Kibria, M.G. Single atom catalysts for selective methane oxidation to oxygenates. *ACS Nano* **2022**, *16*, 8557–8618. [\[CrossRef\]](#)
30. Campo, P.D.; Martinez, C.; Corma, A. Activation and conversion of alkanes in the confined space of zeolite-type materials. *Chem. Soc. Rev.* **2021**, *50*, 8511–8595. [\[CrossRef\]](#)
31. Petrov, A.W.; Ferri, D.; Krumeich, F.; Nachtegaal, M.; Bokhoven, J.A.V.; Krocher, O. Stable complete methane oxidation over palladium based zeolite catalysts. *Nat. Commun.* **2018**, *9*, 2545. [\[CrossRef\]](#)
32. Liu, C.J.; Yu, K.L.; Zhang, Y.P.; Zhu, X.L.; He, F.; Eliasson, B. Characterization of plasma treated Pd/HZSM-5 catalyst for methane combustion. *Appl. Catal. B* **2004**, *47*, 95–100. [\[CrossRef\]](#)
33. Shi, C.K.; Yang, L.F.; Cai, J.X. Cerium promoted Pd/HZSM-5 catalyst for methane combustion. *Fuel* **2007**, *86*, 106–112. [\[CrossRef\]](#)
34. Zhang, Z.S.; Sun, L.W.; Hu, X.F.; Zhang, Y.B.; Tian, H.Y.; Yang, X.G. Anti-sintering Pd@silicalite-1 for methane combustion: Effects of the moisture and SO₂. *Appl. Surf. Sci.* **2019**, *494*, 1044–1054. [\[CrossRef\]](#)
35. Nguyen, T.S.; Mckeever, P.; Arredondo-Arechavala, M.; Wang, Y.C.; Slater, T.J.A.; Haigh, S.J.; Beale, A.M.; Thompson, J.M. Correlation of the ratio of metallic to oxide species with activity of PdPt catalysts for methane oxidation. *Catal. Sci. Technol.* **2020**, *10*, 1408–1421. [\[CrossRef\]](#)
36. Groothaert, M.H.; Smeets, P.J.; Sels, B.F.; Jacobs, P.A.; Schoonheydt, R.A. Selective oxidation of methane by the bis(η-oxo)dicopper core stabilized on ZSM-5 and mordenite zeolites. *J. Am. Chem. Soc.* **2005**, *127*, 1394–1395. [\[CrossRef\]](#)
37. Devos, J.; Bols, M.L.; Plessres, D.; Goethem, C.V.; Seo, J.W.; Hwang, S.J.; Sels, B.F.; Dusselier, M. Synthesis–structure–activity relations in Fe-CHA for C–H activation: Control of Al distribution by interzeolite conversion. *Chem. Mater.* **2020**, *32*, 273–285. [\[CrossRef\]](#)
38. Shah, M.A.; Raynes, S.; Apperley, D.C.; Taylor, R.A. Framework effects on activation and functionalisation of methane in zinc-exchanged zeolites. *ChemPhysChem* **2020**, *21*, 673. [\[CrossRef\]](#)
39. Beznis, N.V.; Laak, A.N.C.V.; Weckhuysen, B.M.; Bitter, J.H. Oxidation of methane to methanol and formaldehyde over Co-ZSM-5 molecular sieves: Tuning the reactivity and selectivity by alkaline and acid treatments of the zeolite ZSM-5 agglomerates. *Microporous Mesoporous Mater.* **2011**, *138*, 176–183. [\[CrossRef\]](#)
40. Lim, J.B.; Jo, D.H.; Hong, S.B. Palladium-exchanged small-pore zeolites with different cage systems as methane combustion catalysts. *Appl. Catal. B* **2017**, *219*, 155–162. [\[CrossRef\]](#)
41. Chen, H.Y.; Lu, J.; Fedeyko, J.M.; Raj, A. Zeolite supported Pd catalysts for the complete oxidation of methane: A critical review. *Appl. Catal. A* **2022**, *633*, 118534. [\[CrossRef\]](#)
42. Zhang, Y.; Glarborg, P.; Andersson, M.P.; Johansen, K.; Torp, T.K.; Jensen, A.D.; Christensen, J.M. Influence of the support on rhodium speciation and catalytic activity of rhodium-based catalysts for total oxidation of methane. *Catal. Sci. Technol.* **2020**, *10*, 6035–6044. [\[CrossRef\]](#)
43. Petrov, A.W.; Ferri, D.; Krocher, O.; Bokhoven, J.A.V. Design of stable palladium-based zeolite catalysts for complete methane oxidation by postsynthesis zeolite modification. *ACS Catal.* **2019**, *9*, 2303–2312. [\[CrossRef\]](#)
44. Zhang, L.L.; Chen, J.F.; Yang, H.L.; Wang, X.H.; Rui, Z.B. In situ mercaptosilane-assisted confinement of Pd nanoparticles in Beta for high-efficient methane oxidation. *Catal. Today* **2022**, *400*, 124–131. [\[CrossRef\]](#)
45. Feng, X.Q.; Wang, T.; Mu, L.; Chen, Z.L.; Liang, J.H.; Xiao, C. Excellent stability for catalytic oxidation of methane over core-shell Pd@silicalite-1 with complete zeolite shell in wet conditions. *Catal. Today* **2022**, *400*, 66–72. [\[CrossRef\]](#)
46. Tang, X.; Lou, Y.; Zhao, R.L.; Tang, B.J.; Guo, W.Y.; Guo, Y.L.; Zhan, W.C.; Jia, Y.Y.; Wang, L.; Dai, S.; et al. Confinement of subnanometric PdCo bimetallic oxide clusters in zeolites for methane complete oxidation. *Chem. Eng. J.* **2021**, *418*, 129398. [\[CrossRef\]](#)
47. Doyle, A.M.; Postolache, R.; Shaw, D.; Rother, R.; Tosheva, L. Methane oxidation over zeolite catalysts prepared from geothermal fluids. *Microporous Mesoporous Mater.* **2019**, *285*, 56–60. [\[CrossRef\]](#)
48. Friberg, I.; Clark, A.H.; Ho, P.H.; Sadokhina, N.; Smales, G.J.; Woo, J.; Auvray, X.; Ferri, D.; Nachtegaal, M.; Krocher, O.; et al. Structure and performance of zeolite supported Pd for complete methane oxidation. *Catal. Today* **2021**, *382*, 3–12. [\[CrossRef\]](#)
49. Yabushita, M.; Yoshida, M.; Muto, F.; Horie, M.; Kunitake, Y.; Nishitoba, T.; Maki, S.; Kanie, K.; Yokoi, T.; Muramatsu, A. Hydrothermal synthesis of Ga-substituted MFI zeolites via a mechanochemical process and their catalytic activity for methane transformation. *Mol. Catal.* **2019**, *478*, 110579. [\[CrossRef\]](#)

50. Losch, P.; Huang, W.X.; Vozniuk, O.; Goodman, E.D.; Schmidt, W.; Cargnello, M. Modular Pd/zeolite composites demonstrating the key role of support hydrophobic/hydrophilic character in methane catalytic combustion. *ACS Catal.* **2019**, *9*, 4742–4753. [[CrossRef](#)]
51. Li, T.; Beck, A.; Krumeich, F.; Artiglia, L.; Ghosalya, M.K.; Roger, M.; Ferri, D.; Krocher, O.; Sushkevich, V.; Safonova, O.V.; et al. Stable palladium oxide clusters encapsulated in silicalite-1 for complete methane oxidation. *ACS Catal.* **2021**, *11*, 7371–7382. [[CrossRef](#)]
52. Gao, M.Y.; Gong, Z.M.; Weng, X.F.; Shang, W.X.; Chai, Y.C.; Dai, W.L.; Wu, G.J.; Guan, N.J.; Li, L.D. Methane combustion over palladium catalyst within the confined space of MFI zeolite. *Chin. J. Catal.* **2021**, *42*, 1689–1699. [[CrossRef](#)]
53. Xiao, C.; Yang, Y.; Meng, D.; Dong, L.; Luo, L.L.; Tan, Z.Y. Stable and active monolithic palladium catalyst for catalytic oxidation of methane using nanozeolite silicalite-1 coating on cordierite. *Appl. Catal. A* **2017**, *531*, 197–202. [[CrossRef](#)]
54. Tang, Z.Y.; Zhang, T.; Luo, D.C.; Wang, Y.J.; Hu, Z.; Yang, R.T. Catalytic combustion of methane: From mechanism and materials properties to catalytic performance. *ACS Catal.* **2022**, *12*, 13457–13474. [[CrossRef](#)]
55. He, L.; Fan, Y.L.; Bellettre, J.; Yue, J.; Luo, L.G. A review on catalytic methane combustion at low temperatures: Catalysts, mechanisms, reaction conditions and reactor designs. *Renew. Sustain. Energy Rev.* **2020**, *119*, 109589. [[CrossRef](#)]
56. Bunting, R.J.; Thompson, J.; Hu, P. The mechanism and ligand effects of single atom rhodium supported on ZSM-5 for the selective oxidation of methane to methanol. *Phys. Chem. Chem. Phys.* **2020**, *22*, 11686–11694. [[CrossRef](#)]
57. Xue, W.J.; Mei, D.H. Mechanistic understanding of methane combustion over H-SSZ-13 zeolite encapsulated palladium nanocluster catalysts. *Chem. Eng. J.* **2022**, *444*, 136671. [[CrossRef](#)]
58. Jørgensen, M.; Gronbeck, H. First-principles microkinetic modeling of methane oxidation over Pd(100) and Pd(111). *ACS Catal.* **2016**, *6*, 6730–6738. [[CrossRef](#)]
59. Bu, X.Y.; Ran, J.Y.; Niu, J.T.; Ou, Z.L.; Tang, L.; Huang, X. Reaction mechanism insights into CH₄ catalytic oxidation on Pt₁₃ cluster: A DFT study. *Mol. Catal.* **2021**, *515*, 111891. [[CrossRef](#)]
60. Wang, T.; Zhang, C.; Wang, J.Y.; Li, H.Y.; Duan, Y.; Liu, Z.; Lee, J.Y.; Hu, X.; Xi, S.B.; Du, Y.H.; et al. The interplay between the suprafacial and intrafacial mechanisms for complete methane oxidation on substituted LaCoO₃ perovskite oxides. *J. Catal.* **2020**, *390*, 1–11. [[CrossRef](#)]
61. Saracco, G.; Geobaldo, F.; Baldi, G. Methane combustion on Mg-doped LaMnO₃ perovskite catalysts. *Appl. Catal. B* **1999**, *20*, 277–288. [[CrossRef](#)]
62. Ciuparu, D.; Altman, E.; Pfefferle, L. Contributions of lattice oxygen in methane combustion over PdO-based catalysts. *J. Catal.* **2001**, *203*, 64–74. [[CrossRef](#)]
63. Stotz, H.; Maier, L.; Boubnov, A.; Gremminger, A.T.; Grunwaldt, J.D.; Deutschmann, O. Surface reaction kinetics of methane oxidation over PdO. *J. Catal.* **2019**, *370*, 152–175. [[CrossRef](#)]
64. Hu, W.D.; Shao, Z.J.; Cao, X.M.; Hu, P. Multi sites vs single site for catalytic combustion of methane over Co₃O₄(110): A first-principles kinetic Monte Carlo study. *Chin. J. Catal.* **2020**, *41*, 1369–1377. [[CrossRef](#)]
65. Tao, F.F.; Shan, J.J.; Nguyen, L.; Wang, Z.Y.; Zhang, S.R.; Zhang, L.; Wu, Z.L.; Huang, W.X.; Zeng, S.B.; Hu, P. Understanding complete oxidation of methane on spinel oxides at a molecular level. *Nat. Commun.* **2015**, *6*, 7798. [[CrossRef](#)]
66. Zhu, J.; Sushkevich, V.L.; Knorpp, A.J.; Newton, M.A.; Mizuno, S.C.M.; Wakihara, T.; Okubo, T.; Liu, Z.D.; Bokhoven, J.A.V. Cu-erionite zeolite achieves high yield in direct oxidation of methane to methanol by isothermal chemical looping. *Chem. Mater.* **2020**, *32*, 1448–1453. [[CrossRef](#)]
67. Brezicki, G.; Zheng, J.; Paolucci, C.; Schlogl, R.; Davis, R.J. Effect of the Co-cation on Cu speciation in Cu-exchanged mordenite and ZSM-5 catalysts for the oxidation of methane to methanol. *ACS Catal.* **2021**, *11*, 4973–4987. [[CrossRef](#)]
68. Yu, T.; Li, Z.; Jones, W.; Liu, Y.S.; He, Q.; Song, W.Y.; Du, P.F.; Yang, B.; An, H.Y.; Farmer, D.M.; et al. Identifying key mononuclear Fe species for low-temperature methane oxidation. *Chem. Sci.* **2021**, *12*, 3152–3160. [[CrossRef](#)]
69. Tabor, E.; Dedecek, J.; Mlekodaj, K.; Sobalik, Z.; Andrikopoulos, P.C.; Sklenak, S. Dioxygen dissociation over man-made system at room temperature to form the active α -oxygen for methane oxidation. *Sci. Adv.* **2020**, *6*, 9776. [[CrossRef](#)]
70. Kim, M.S.; Park, E.D. Aqueous-phase partial oxidation of methane with H₂O₂ over Fe-ZSM-5 catalysts prepared from different iron precursors. *Microporous Mesoporous Mater.* **2021**, *324*, 111278. [[CrossRef](#)]
71. Sun, S.M.; Barnes, A.J.; Gong, X.X.; Lewis, R.J.; Dummer, N.F.; Bere, T.; Shaw, G.; Richards, N.; Morgan, D.J.; Hutchings, G.J. Lanthanum modified Fe-ZSM-5 zeolites for selective methane oxidation with H₂O₂. *Catal. Sci. Technol.* **2021**, *11*, 8052–8064. [[CrossRef](#)]
72. Snyder, B.E.R.; Bols, M.L.; Rhoda, H.M.; Plessers, D.; Schoonheydt, R.A.; Sels, B.F.; Solomon, E.I. Cage effects control the mechanism of methane hydroxylation in zeolites. *Science* **2021**, *373*, 327–331. [[CrossRef](#)]
73. Dinh, K.T.; Sullivan, M.M.; Narsimhan, K.; Serna, P.; Meyer, R.J.; Dinca, M.; Román-Leshkov, Y. Continuous partial oxidation of methane to methanol catalyzed by diffusion-paired copper dimers in copper-exchanged zeolites. *J. Am. Chem. Soc.* **2019**, *141*, 11641–11650. [[CrossRef](#)]
74. Yang, J.Y.; Du, X.R.; Qiao, B.T. Methane oxidation to methanol over copper-containing zeolite. *Chem* **2021**, *7*, 2270–2272. [[CrossRef](#)]
75. Park, M.B.; Ahn, S.H.; Mansouri, A.; Ranocchiari, M.; Bokhoven, J.A.V. Comparative study of diverse copper zeolites for the conversion of methane into methanol. *ChemCatChem* **2017**, *9*, 3705. [[CrossRef](#)]
76. Ravi, M.; Ranocchiari, M.; Bokhoven, J.A.V. The direct catalytic oxidation of methane to methanol—A critical assessment. *Angew. Chem. Int. Ed.* **2017**, *56*, 16464. [[CrossRef](#)]

77. Pappas, D.K.; Borfecchia, E.; Dyballa, M.; Pankin, I.A.; Lomachenko, K.A.; Martini, A.; Signorile, M.; Teketel, S.; Arstad, B.; Berlier, G.; et al. Methane to methanol: Structure–activity relationships for Cu-CHA. *J. Am. Chem. Soc.* **2017**, *139*, 14961–14975. [[CrossRef](#)]
78. Szecsenyi, A.; Li, G.; Gascon, J.; Pidko, E.A. Mechanistic complexity of methane oxidation with H₂O₂ by single-site Fe/ZSM-5 catalyst. *ACS Catal.* **2018**, *8*, 7961–7972. [[CrossRef](#)]
79. Li, S.C.; Wang, Y.J.; Wu, T.; Schneider, W.F. First-principles analysis of site- and condition-dependent Fe speciation in SSZ-13 and implications for catalyst optimization. *ACS Catal.* **2018**, *8*, 10119–10130. [[CrossRef](#)]
80. Alayon, E.M.C.; Nachttegaal, M.; Bodi, A.; Bokhoven, J.A.V. Reaction conditions of methane-to-methanol conversion affect the structure of active copper sites. *ACS Catal.* **2014**, *4*, 16–22. [[CrossRef](#)]
81. Han, B.Z.; Yang, Y.; Xu, Y.Y.; Etim, U.J.; Qiao, K.; Xu, B.J.; Yan, Z.F. A review of the direct oxidation of methane to methanol. *Chin. J. Catal.* **2016**, *37*, 1206–1215. [[CrossRef](#)]
82. Wang, X.X.; Wang, Y.; Tang, Q.H.; Guo, Q.; Zhang, Q.H.; Wan, H.L. MCM-41-supported iron phosphate catalyst for partial oxidation of methane to oxygenates with oxygen and nitrous oxide. *J. Catal.* **2003**, *217*, 457–467. [[CrossRef](#)]
83. Wang, Y.; Wang, X.X.; Su, Z.; Guo, Q.; Tang, Q.H.; Zhang, Q.H.; Wan, H.L. SBA-15-supported iron phosphate catalyst for partial oxidation of methane to formaldehyde. *Catal. Today* **2004**, *93*, 155–161. [[CrossRef](#)]
84. Ruddy, D.A.; Ohler, N.L.; Bell, A.T.; Tilley, T.D. Thermolytic molecular precursor route to site-isolated vanadia–silica materials and their catalytic performance in methane selective oxidation. *J. Catal.* **2006**, *238*, 277–285. [[CrossRef](#)]
85. Nguyen, L.D.; Lorient, S.; Launay, H.; Pigamo, A.; Dubois, J.L.; Millet, J.M.M. Study of new catalysts based on vanadium oxide supported on mesoporous silica for the partial oxidation of methane to formaldehyde: Catalytic properties and reaction mechanism. *J. Catal.* **2006**, *237*, 38–48. [[CrossRef](#)]
86. An, D.L.; Zhang, Q.H.; Wang, Y. Copper grafted on SBA-15 as efficient catalyst for the selective oxidation of methane by oxygen. *Catal. Today* **2010**, *157*, 143–148. [[CrossRef](#)]
87. Li, Y.; An, D.L.; Zhang, Q.H.; Wang, Y. Copper-catalyzed selective oxidation of methane by oxygen: Studies on catalytic behavior and functioning mechanism of CuO_x/SBA-15. *J. Phys. Chem. C* **2008**, *112*, 13700–13708. [[CrossRef](#)]
88. Zhu, K.X.; Liang, S.X.; Cui, X.J.; Huang, R.; Wan, N.B.; Hua, L.; Li, H.Y.; Chen, H.Y.; Zhao, Z.C.; Hou, G.J.; et al. Highly efficient conversion of methane to formic acid under mild conditions at ZSM-5-confined Fe-sites. *Nano Energy* **2021**, *82*, 105718. [[CrossRef](#)]
89. Wang, V.C.C.; Maji, S.; Chen, P.P.Y.; Lee, H.K.; Yu, S.S.F.; Chan, S.I. Alkane oxidation: Methane monooxygenases, related enzymes, and their biomimetics. *Chem. Rev.* **2017**, *117*, 8574–8621. [[CrossRef](#)]
90. Qi, G.D.; Davies, T.E.; Nasrallah, A.; Sainna, M.A.; Howe, A.G.R.; Lewis, R.J.; Quesne, M.; Catlow, C.R.A.; Willock, D.J.; He, Q.; et al. Au-ZSM-5 catalyses the selective oxidation of CH₄ to CH₃OH and CH₃COOH using O₂. *Nat. Catal.* **2022**, *5*, 45–54. [[CrossRef](#)]
91. Li, H.Y.; Fei, M.C.; Troiano, J.L.; Ma, L.; Yan, X.X.; Tieu, P.; Yuan, Y.C.; Zhang, Y.H.; Liu, T.Y.; Pan, X.Q.; et al. Selective Methane Oxidation by Heterogenized Iridium Catalysts. *J. Am. Chem. Soc.* **2023**, *145*, 769–773. [[CrossRef](#)]
92. Pannov, G.I.; Sobolev, V.I.; Kharitonov, A.S. The role of iron in N₂O decomposition on ZSM-5 zeolite and reactivity of the surface oxygen formed. *J. Mol. Catal.* **1990**, *61*, 85–97. [[CrossRef](#)]
93. Sobolev, V.I.; Panov, G.I.; Kharitonov, A.S.; Romannikov, V.N.; Volodin, A.M.; Ione, K.G. Catalytic properties of ZSM-5 zeolites in N₂O decomposition: The role of iron. *J. Catal.* **1993**, *139*, 435–443. [[CrossRef](#)]
94. Dubkov, K.A.; Sobolev, V.I.; Talsi, E.P.; Rodkin, M.A.; Watkins, N.H.; Shteinman, A.A.; Panov, G.I. Kinetic isotope effects and mechanism of biomimetic oxidation of methane and benzene on FeZSM-5 zeolite. *J. Mol. Catal. A* **1997**, *123*, 155–161. [[CrossRef](#)]
95. Dinh, K.T.; Sullivan, M.M.; Serna, P.; Meyer, R.J.; Dinca, M.; Roman-Leshkov, Y. Viewpoint on the partial oxidation of methane to methanol using Cu- and Fe-exchanged zeolites. *ACS Catal.* **2018**, *8*, 8306–8313. [[CrossRef](#)]
96. Yu, T.; Su, Y.; Wang, A.Q.; Weckhuysen, B.M.; Luo, W.H. Efficient synthesis of monomeric Fe species in zeolite ZSM-5 for the low-temperature oxidation of methane. *ChemCatChem* **2021**, *13*, 2766–2770. [[CrossRef](#)]
97. Citek, C.; Gary, J.B.; Wasinger, E.C.; Stack, T.D.P. Chemical plausibility of Cu(III) with biological ligation in pMMO. *J. Am. Chem. Soc.* **2015**, *137*, 6991–6994. [[CrossRef](#)]
98. Bols, M.L.; Hallaert, S.D.; Snyder, B.E.R.; Devos, J.; Plessers, D.; Rhoda, H.M.; Dusselier, M.; Schoonheydt, R.A.; Pierloot, K.; Solomon, E.I.; et al. Spectroscopic identification of the α-Fe/α-O active site in Fe-CHA zeolite for the low-temperature activation of the methane C–H bond. *J. Am. Chem. Soc.* **2018**, *140*, 12021–12032. [[CrossRef](#)]
99. Snyder, B.E.R.; Vanelderden, P.; Bols, M.L.; Hallaert, S.D.; Bottger, L.H.; Ungur, L.; Pierloot, K.; Schoonheydt, R.A.; Sels, B.F.; Solomon, E.I. The active site of low-temperature methane hydroxylation in iron-containing zeolites. *Nature* **2016**, *536*, 317–321. [[CrossRef](#)]
100. Mahyuddin, M.H.; Tanaka, T.; Shiota, Y.; Staykov, A.; Yoshizawa, K. Methane partial oxidation over [Cu₂(μ-O)]²⁺ and [Cu₃(μ-O)₃]²⁺ active species in large-pore zeolites. *ACS Catal.* **2018**, *8*, 1500–1509. [[CrossRef](#)]
101. Li, G.; Vassilev, P.; Sanchez-Sanchez, M.; Lercher, J.A.; Hensen, E.J.M.; Pidko, E.A. Stability and reactivity of copper oxo-clusters in ZSM-5 zeolite for selective methane oxidation to methanol. *J. Catal.* **2016**, *338*, 305–312. [[CrossRef](#)]
102. Heyer, A.J.; Plessers, D.; Braun, A.; Rhoda, H.M.; Bols, M.L.; Hedman, B.; Hodgson, K.O.; Schoonheydt, R.A.; Sels, B.F.; Solomon, E.I. Methane activation by a mononuclear copper active site in the zeolite mordenite: Effect of metal nuclearity on reactivity. *J. Am. Chem. Soc.* **2022**, *144*, 19305–19316. [[CrossRef](#)] [[PubMed](#)]
103. Sushkevich, V.L.; Palagin, D.; Ranocchiaro, M.; Bokhoven, J.A.V. Selective anaerobic oxidation of methane enables direct synthesis of methanol. *Science* **2017**, *356*, 523–527. [[CrossRef](#)] [[PubMed](#)]

104. Newton, M.A.; Knorpp, A.J.; Sushkevich, V.L.; Palagin, D.; Bokhoven, J.A.V. Active sites and mechanisms in the direct conversion of methane to methanol using Cu in zeolitic hosts: A critical examination. *Chem. Soc. Rev.* **2020**, *49*, 1449–1486. [[CrossRef](#)]
105. Wulfers, M.J.; Teketel, S.; Lpek, B.; Lobo, R.F. Conversion of methane to methanol on copper-containing small-pore zeolites and zeotypes. *Chem. Commun.* **2015**, *51*, 4447–4450. [[CrossRef](#)]
106. Kulkarni, A.R.; Zhao, Z.J.; Siahrostami, S.; Nørskov, J.K.; Studt, F. Monocopper active site for partial methane oxidation in Cu-exchanged 8MR zeolites. *ACS Catal.* **2016**, *6*, 6531–6536. [[CrossRef](#)]
107. Sushkevich, V.L.; Palagin, D.; Bokhoven, J.A.V. The effect of the active-site structure on the activity of copper mordenite in the aerobic and anaerobic conversion of methane into methanol. *Angew. Chem. Int. Ed.* **2018**, *57*, 8906. [[CrossRef](#)]
108. Liu, N.; Li, Y.; Dai, C.N.; Xu, R.N.; Yu, G.Q.; Wang, N.; Chen, B.H. H₂O in situ induced active site structure dynamics for efficient methane direct oxidation to methanol over Fe-BEA zeolite. *J. Catal.* **2022**, *414*, 302–312. [[CrossRef](#)]
109. Adeyiga, O.; Odoh, S.O. Methane over-oxidation by extra-framework copper-oxo active sites of copper-exchanged zeolites: Crucial role of traps for the separated methyl group. *ChemPhysChem* **2021**, *22*, 1101. [[CrossRef](#)]
110. Lucas, A.D.; Valverde, J.L.; Rodriguez, L.; Sanchez, P.; Garcia, M.T. Partial oxidation of methane to formaldehyde over Mo/HZSM-5 catalysts. *Appl. Catal. A* **2000**, *203*, 81–90. [[CrossRef](#)]
111. Hammond, C.; Jenkins, R.L.; Dimitratos, N.; Lopez-Sanchez, J.A.; Rahim, M.H.; Forde, M.M.; Thetford, A.; Murphy, D.M.; Hagen, H.; Stangland, E.E.; et al. Catalytic and mechanistic insights of the low-temperature selective oxidation of methane over Cu-promoted Fe-ZSM-5. *Chem. Eur. J.* **2012**, *18*, 15735–15745. [[CrossRef](#)]
112. Yang, N.T.; Ren, Z.L.; Yang, C.G.; Wu, P.; Zeng, G.F. Direct oxidation of CH₄ to HCOOH over extra-framework stabilized Fe@MFI catalyst at low temperature. *Fuel* **2021**, *305*, 121624. [[CrossRef](#)]
113. Shahami, M.; Shantz, D.F. Zeolite acidity strongly influences hydrogen peroxide activation and oxygenate selectivity in the partial oxidation of methane over M,Fe-MFI (M: Ga, Al, B) zeolites. *Catal. Sci. Technol.* **2019**, *9*, 2945–2951. [[CrossRef](#)]
114. Hammond, C.; Forde, M.M.; Rahim, M.H.A.; Thetford, A.; He, Q.; Jenkins, R.L.; Dimitratos, N.; Lopez-Sanchez, J.A.; Dummer, N.F.; Murphy, D.M.; et al. Direct catalytic conversion of methane to methanol in an aqueous medium by using copper-promoted Fe-ZSM-5. *Angew. Chem. Int. Ed.* **2012**, *51*, 5129–5133. [[CrossRef](#)]
115. Yu, X.; Wu, B.; Huang, M.; Lu, Z.X.; Li, J.; Zhong, L.S.; Sun, Y.H. IrFe/ZSM-5 synergistic catalyst for selective oxidation of methane to formic acid. *Energy Fuels* **2021**, *35*, 4418–4427. [[CrossRef](#)]
116. Narsimhan, K.; Michaelis, V.K.; Mathies, G.; Gunther, W.R.; Griffin, R.G.; Roman-Leshkov, Y. Methane to acetic acid over Cu-exchanged zeolites: Mechanistic insights from a site-specific carbonylation reaction. *J. Am. Chem. Soc.* **2015**, *137*, 1825–1832. [[CrossRef](#)]
117. Wang, X.M.; Qi, G.D.; Xu, J.; Li, B.J.; Wang, C.; Deng, F. NMR-spectroscopic evidence of intermediate-dependent pathways for acetic acid formation from methane and carbon monoxide over a ZnZSM-5 zeolite catalyst. *Angew. Chem. Int. Ed.* **2012**, *51*, 3850–3853. [[CrossRef](#)]
118. Fang, Z.H.; Huang, M.Y.; Liu, B.; Chen, J.; Jiang, F.; Xu, Y.B.; Liu, X.H. Insights into Fe species structure-performance relationship for direct methane conversion toward oxygenates over Fe-MOR catalysts. *ChemCatChem* **2022**, *14*, e202200218. [[CrossRef](#)]

Disclaimer/Publisher's Note: The statements, opinions and data contained in all publications are solely those of the individual author(s) and contributor(s) and not of MDPI and/or the editor(s). MDPI and/or the editor(s) disclaim responsibility for any injury to people or property resulting from any ideas, methods, instructions or products referred to in the content.